Service Contract on
Monitoring and Assessment
of Sectorial Implementation Actions
(ENV.C.3/SER/2011/0009)

Modelling compliance with NO_2 and PM10 air quality limit values in the GAINS model

TSAP Report #9

Version 1.0

Gregor Kiesewetter[1], Jens Borken-Kleefeld[1], Wolfgang Schöpp[1],
Chris Heyes[1], Imrich Bertok[1], Philippe Thunis[2],
Bertrand Bessagnet[3], Etienne Terrenoire[3], Markus Amann[1]

[1] International Institute for Applied Systems Analysis IIASA

[2] Joint Research Centre JRC-IES

[3] INERIS

March 2013

The authors

Gregor Kiesewetter, Jens Borken-Kleefeld, Wolfgang Schöpp, Chris Heyes, Imrich Bertok, and Markus Amann are working at the International Institute for Applied Systems Analysis (IIASA), Laxenburg, Austria. Philippe Thunis is working at the Joint Research Centre- Institute for Environment and Sustainability (JRC-IES) of the European Commission, Ispra, Italy. Bertrand Bessagnet and Etienne Terrenoire are working at the Institut National de l'Environnement Industriel et des Risques (INERIS), Paris, France.

Acknowledgements

This report was produced under the Service Contract on Monitoring and Assessment of Sectorial Implementation Actions (ENV.C.3/SER/2011/0009) of DG-Environment of the European Commission.

The methodology was developed within the EC4MACS (European Consortium for the Modelling of Air pollution and Climate Strategies) project with financial contributions of the LIFE financial instrument of the European Community.

Monitoring data used in this project were obtained from the European air quality database (AirBase) maintained by the European Environment Agency (EEA). French PM10 monitoring data were partly provided by INERIS.

The authors would like to thank John Stedman for detailed comments that helped to improve the report.

Disclaimer

More information on the web

More information about the methodology of the GAINS (Greenhouse gas – Air pollution INteractions and Synergies) integrated assessment model and interactive access to input data and results is available on-line: http://gains.iiasa.ac.at/TSAP.

Summary

EU Member States are currently facing considerable difficulties in complying with air quality limit values for traffic related air pollutants such as NO_2 and PM10. As part of IIASA's input to the revision of the EU air policy, the effects of future emission control scenarios on compliance with limit values at the local level are assessed. This report introduces the methodology that has been developed to downscale results from the GAINS integrated assessment model to derive concentration estimates at individual air quality monitoring stations. The methodology builds on a combination of bottom up modelling and analysis of monitoring data for the year 2009. Different components of the measured concentrations are explained to the extent possible for the past, and then modelled for the future.

For roadside monitoring stations, a basic distinction is made between observed background concentrations and the residual increment, mainly from traffic sources. The background is composed of a regional background component modelled with linear source receptor relations derived with the EMEP model, plus an urban scale increment that is derived from a model run with the CHIMERE model with approximately 7km×7km resolution. The roadside increment is explained and modelled with simplified box models containing NO_x-O_3 photochemistry at NO_2 monitoring stations, and passive dispersion of primary PM emissions at PM10 monitoring stations.

Our modelling approach enables concentration estimates for more than 2000 NO_2 monitoring stations and more than 1900 PM10 monitoring stations in the EU, including some 330 NO_2 and 130 PM10 traffic stations, and a large fraction (67% / 80%) of the stations exceeding limit values in 2009.

Modelling such a large number of stations requires simplifications, as some critical input data (e.g., local fleet composition, driving modes, emission trends, etc.) is unavailable for all stations at the European scale. While simplifying assumptions (e.g., that individual stations follow national trends) introduce inaccuracies for individual stations, results that are more robust can be obtained by a statistical analysis of more aggregated results. For this purpose, we sort stations into compliance classes according to their modelled concentrations and treat the number of stations in each category as a more robust outcome than predictions for individual stations.

Modelled results are validated against AirBase observations for the years 2000-2008. The model is able to reproduce past trends well, particularly when cumulative results are analysed.

The methodology described here provides for the first time the possibility to derive within the GAINS model quantitative estimates of the effects of EU-wide air policy measures on air quality at the street level, and to assess the interplay between EU-wide, national, and local measures for the attainment of air quality limit values.

Table of Contents

List of Acronyms

CTM	Chemistry Transport Model
EMEP	European Monitoring and Evaluation Programme
EU	European Union
EU27	27 Member States of the European Union
GAINS	Greenhouse gas – Air pollution INteractions and Synergies
NH_3	Ammonia
NO	Nitrogen monoxide
NO_2	Nitrogen dioxide
NO_x	Reactive nitrogen family of species, $NO_x = NO + NO_2$
O_3	Ozone
PM10	Particulate matter, aerodynamic diameter less than 10 µm
PM2.5	Particulate matter, aerodynamic diameter less than 2.5 µm
PM_{coarse}	Particulate matter, aerodynamic diameter 2.5µm – 10 µm
SNAP	Selected Nomenclature for Air Pollution
SO_2	Sulphur dioxide
VOC	Non-methane volatile organic compounds

1 Introduction

As an input to the review and revision of the EU air policy in 2013, the GAINS[1] model is employed to provide an outlook into the likely development of air quality that can be envisaged from the latest expectations on economic development and the implementation of recent policies on energy, transport, agriculture and climate change (Amann et al. 2012a; Amann et al. 2012b).

The GAINS model, as an integrated assessment model, brings together information on the sources and impacts of air pollutant and greenhouse gas emissions and their interactions (Amann et al. 2011). GAINS addresses air pollution impacts on human health from fine particulate matter and ground-level ozone, vegetation damage caused by ground-level ozone, the acidification of terrestrial and aquatic ecosystems and excess nitrogen deposition of soils, in addition to the mitigation of greenhouse gas emissions. For the revision of the EU air policy, additional emission control measures are explored that could reduce actual damage from these effects in cost-effective ways.

As the overall magnitude of health and environmental damages in Europe is strongly influenced by the large-scale exposure of European population and ecosystems to air pollution from local as well as more distant emission sources, the GAINS analysis adopts a European-wide perspective and quantifies exposure at a 28km×28km spatial resolution for ecosystems and 7km×7km for human health.

Member States are currently faced with wide-spread compliance problems with the EU air quality limit values for NO_2 and PM10. Compliance with limit values needs to be achieved at all monitoring stations, in particular including those at the street level, where ambient concentrations are influenced not only by long-range transported pollution from European background, but largely by local emission sources.

Obviously, a 28km×28km spatial resolution will not be sufficient to judge how changes in future emissions would affect compliance with the air quality limit values at the street level.

To assess the interplay between local and Europe-wide emission control measures on compliance, this report introduces a new methodology to downscale GAINS results obtained for the 28km spatial resolution to individual air quality monitoring sites for which data have been reported to the AirBase system of the European Environment Agency (EEA)[2].

The modeling scheme relies on a combination of observational data and bottom up modeling. It provides concentration estimates for all AirBase monitoring stations that fulfill a few basic data coverage criteria in the base year 2009. For background

[1] Greenhouse gas – Air pollution Interactions and Synergies

[2] http://acm.eionet.europa.eu/databases/airbase/

stations that are not directly influenced by local road traffic emissions, the 7km×7km grid results are taken. In addition to this, the model calculates for roadside AirBase stations the differences in observed concentrations to the measurements at the nearest background observation sites, and relates them to corresponding emissions as modeled in GAINS. This makes it possible to modify the contributions of the different source types for future emission control scenarios. The methodology builds on work conducted under the EC4MACS project of the LIFE program (www.ec4macs.eu), bringing together results from IIASA's GAINS integrated assessment model, the CHIMERE atmospheric chemistry model of INERIS (France), and the COPERT model of the Aristotle University Thessaloniki (Greece). JRC-IES provided valuable assistance by preparing and analysing model results and monitoring data.

The remainder of this report is organized as follows: In Chapter 2 the downscaling methodology is introduced for the urban background part (Section 2.3) and traffic stations (Section 2.4). Results are validated against observations in Chapter 3. Chapter 4 reviews uncertainties, followed by a general discussion and conclusions in Chapter 5.

2 Methodology

2.1 Overview

Impact calculations in GAINS rely on linear transfer coefficients calculated with the EMEP chemistry transport model (Simpson et al. 2012, www.emep.int), currently available at a resolution of 0.5° (lon) ×0.25° (lat) or roughly 28km×28km. This resolution is sufficient to describe large scale impacts, but already concentrations measured at urban background sites (i.e. stations not directly influencedby local traffic) exceed 28km grid average values significantly and hence require finer model resolution. Traffic-related air pollutants such as nitrogen dioxide (NO_2) and particulate matter (PM) show roadside concentrations that are again significantly higher than urban background values and thus require an even more detailed modeling.

Our modeling scheme consists of several steps built on each other. Essentially, we treat a roadside concentration as being composed of an appropriate background[3] plus a roadside increment due to local traffic,

$$roadside\ concentration = background + traffic\ increment$$

where the "background" is itself composed of a large scale background and an urban increment (see Figure 2.1). The different contributions are diagnosed from observations for the base year 2009 and explained to the extent possible with the models available.

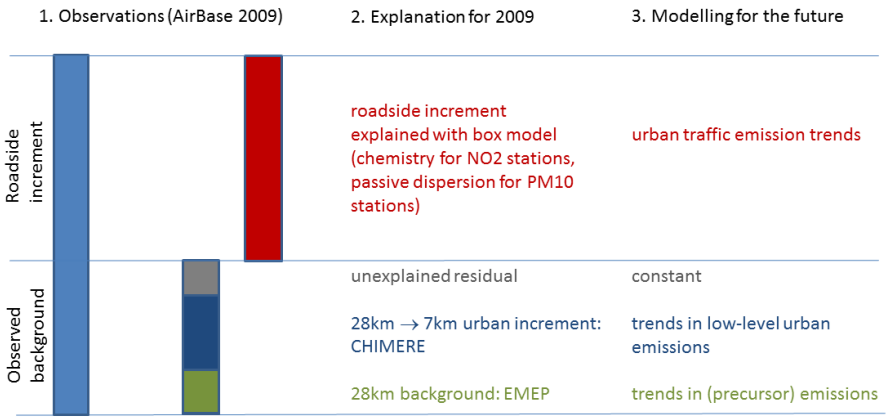

Figure 2.1: Schematic explanation of the different components in roadside observations and how they are represented in the traffic station module.

[3] Measured background concentrations are calculated as the average of all available background sites with the same area type as the roadside station ("urban", "suburban", "rural") in the same city or a radius of 20km around the traffic station.

For future emission scenarios, we modify each component following the change in related emissions. A schematic overview of the model is displayed in Figure 2.1.

In detail, the observed background to any roadside station is modeled from the following components:

- A regional background component, essentially from regional and long-range transported anthropogenic and natural emissions. This is modeled in GAINS for the past and for future scenarios with the source-receptor relationships derived from the EMEP model with a 28km×28km spatial resolution.
- An urban background increment, assumed to emerge from low-level (transport and heating) emission sources within the city. This is derived from a downscaling of the 28km×28km model results to a 7km×7km resolution using the fine-scale concentration patterns developed with the CHIMERE model, based on the fine scale emission inventory of local low level sources. The emission inventory is described in Appendix A, and a detailed description of the CHIMERE model is given in Appendix B. The resulting average concentration for each 7km×7km grid cell is then apportioned to an urban and a sub-urban zone, based on population density (according to the position of the roadside station, either the urban or the sub-urban 7×7km concentration is used as appropriate background). For future scenarios this increment is modified following the changes in the relevant low-level emissions.
- The residual part, i.e., the difference between the modeled and observed urban background concentration. This fraction remains unexplained by the available models, and is kept constant for future scenarios as a conservative estimate. If model results overestimate observed background concentrations for the past, modeled values are scaled with a constant factor to match observations in the base year.

The roadside increment of an AirBase street station is determined from the difference to the corresponding observed background concentration. This difference is assumed to result from traffic sources within the street canyon, although their emissions strengths are unknown. The roadside increment is modeled as follows:

- For stations monitoring NO_2, the observed roadside increment is explained with a simple box model of the $NO/NO_2/O_3$ chemistry. Regression with past observations of the observed roadside increments allows for each station estimating the characteristic residence time of air in the street canyon. With this station-specific residence time, future NO_2 increments can then be calculated for any emission scenario.

- PM10: As only very few station pairs provide data for PM2.5 roadside increments, the fine fraction of the roadside increment is estimated by scaling the observed NO_x increment with the PM2.5/NO_x ratio of traffic emissions in a country. Such a scaling assumes that the mixing characteristics of PM2.5 are similar to those of a passive gas, e.g., those of NO_x that have been determined in the preceding step. For future scenarios, the PM2.5 increment is assumed to follow the trend in urban traffic emissions of PM2.5 in a country. The remaining difference to the observed PM10 roadside increment is then assumed to consist of PM_{coarse}, i.e., PM between 2.5 and 10 µm, mainly from primary emissions of PM_{coarse} from traffic sources (tire and brake wear, road abrasion) and re-suspension. In absence of relevant emission legislation, these components are assumed to follow the future trend in urban traffic volumes.

The different components are determined for the year 2009 using AirBase observations, emissions and meteorology for this year, and then validated by a back-casting for the years 2000-2008.

For any AirBase station that is classified as background station, the same scheme is applied, but without any calculation of a roadside increment. In this case, the concentration measured at the station itself (rather than the average background, as for a roadside station) is explained by the sum of regional (28km) background (EMEP), 28km to 7km increment (CHIMERE), and the unexplained residual.

Altogether, the modeling scheme provides results for more than 2000 NO_2 monitoring stations and more than 1900 PM10 monitoring stations, among them a large fraction of the critical stations currently exceeding air quality limit values. Only annual mean concentrations are modeled. Since also short-term limit values exist, we use statistical relations between the annual mean and the n^{th} highest value to model compliance with the short term limit values. These relations are described in detail in Section 2.2.

The modeling of background concentrations outlined above is discussed in detail in Section 2.3, and the traffic increment models for NO_2 and PM10 are described in Section 2.4.

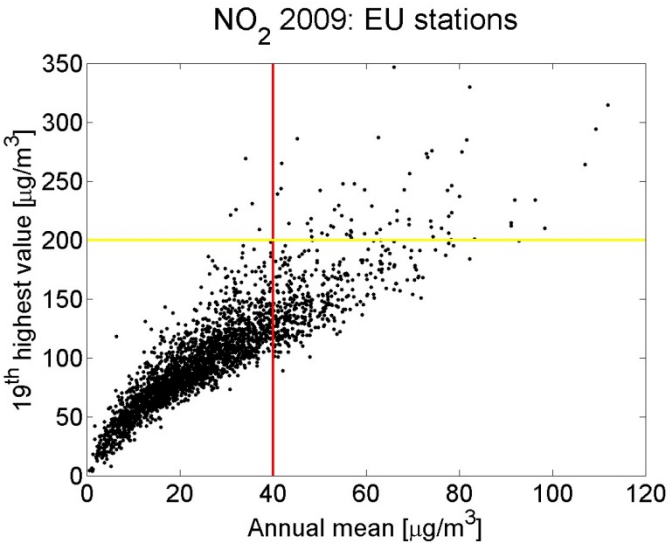

Figure 2.2. Annual mean versus 19th highest hourly value of NO_2 concentrations at all measurement stations in AirBase 2009. Hourly and annual limit values are indicated as yellow and red lines, respectively. Out of more than 60 stations violating the hourly limit value, only six do not exceed the annual mean limit value.

2.2 The relation between limit values for annual mean concentrations and daily/hourly exceedances

Legally binding limit values for ground-level concentrations of NO_2 and PM10 have been set forth in the EU Air Quality Directive (2008/50/EC). Both pollutants have two different limit values associated with different averaging periods: a short-time limit value accompanied by an allowed number of exceedances per year, and a limit value on annual mean concentrations. In case of NO_2, the short-term limit value refers to hourly average concentrations, with a limit of 200µg/m^3 and 18 allowed exceedances per year, while for PM10 the short-term limit value refers to daily mean concentrations, with a limit of 50µg/m^3 not to be exceeded more than 35 times per year. The annual mean limit value is set to 40µg/m^3 for both pollutants. Member States are required to establish compliance with all of these limit values, and thus all of them are explicitly or implicitly included in our assessment. Practice has shown that the different types of limit values confront Member States with different levels of difficulty to meet them. In case of NO_2, the annual mean limit value of 40µg/m^3 is in most cases a more stringent target than the hourly limit value: Only very few stations exceed the hourly limit value without violating the annual mean limit value (see Figure 2.2). In the case of PM10, the limit on daily exceedances is more difficult to attain than the annual mean limit value of 40µg/m^3.

To provide robust results, our modeling scheme is designed to give predictions of annual mean concentration values rather than daily or even hourly values. In our analysis, we focus on the assessment of compliance with the more stringent limit value for each pollutant. In the case of NO_2, assessing compliance with the annual mean limit value of 40µg/m^3 is sufficient for this purpose. For PM10, the critical limit value is the one on daily means with 35 allowed exceedance days. Here we utilize the fact that a strong linear relation exists between the 36th highest daily value and the annual mean concentration, so that the limit value on daily exceedances can be represented well by an equivalent lower limit value on the annual mean of 30µg/m^3 (see Figure 2.3). Hence we are able to provide estimates for compliance with all limit values on NO_2 and PM10, even though only annual mean concentration values are calculated.

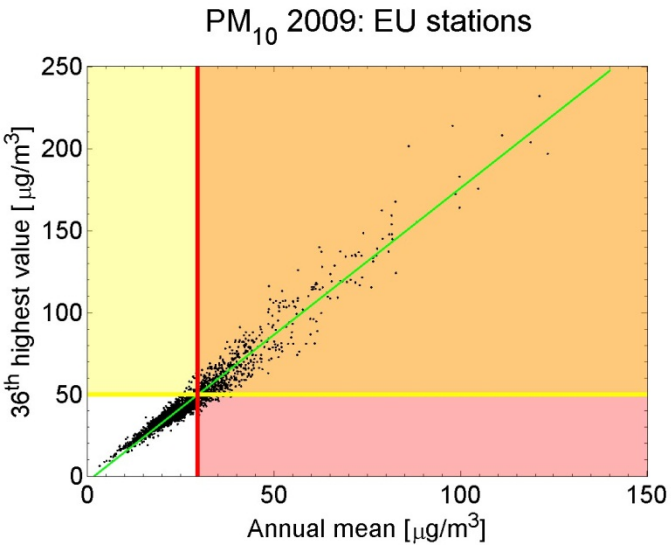

Figure 2.3: Annual mean vs. 36th highest daily value of PM10 at all AirBase stations in 2009. Yellow line: daily limit value, red line: modified annual mean limit value (30µg/m^3) that matches the daily limit value.

2.3 Modelling urban background concentrations

Long-range and transboundary transport of air pollution is represented in the GAINS model through linear transfer coefficients that have been derived from calculations with the EMEP model (Simpson et al. 2012) at a resolution of 0.5° (lon) × 0.25° (lat) or roughly 28×28km.

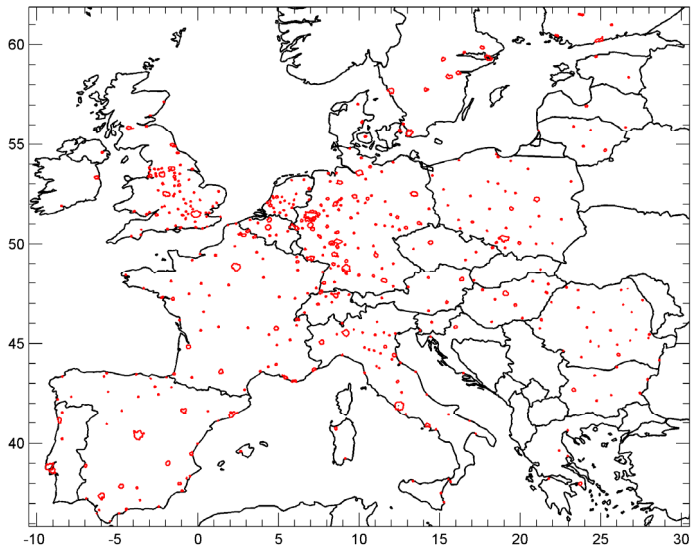

Figure 2.4. Extent of the CHIMERE model domain. Urban polygons for which a further disaggregation of the 7×7km grid results into urban and suburban part is made are shown in red.

In this linearized scheme, concentrations c_{NOx} in the receptor grid cell $\boldsymbol{i} = \begin{pmatrix} i_{lon} \\ i_{lat} \end{pmatrix}$ are calculated as

$$c_{NOx}(\boldsymbol{i}) = \delta_{NOx}(\boldsymbol{i}) + \sum_{r=1}^{n_r} E_{NOx}(r) \cdot \nu(\boldsymbol{i}, r) \qquad (2.1)$$

Here E_{NOx} denotes country total NO_x emissions originating from source region r $(r = 1 \dots n_r)$, which are multiplied by the NO_x transfer coefficient ν that describes the NO_x concentration in grid $\boldsymbol{i}$ resulting from emissions in r, and summed over all source regions. In the current version of source receptor calculations, 53 source regions are included (EU27, Switzerland, Norway, Croatia, Iceland, Serbia and Montenegro, Belarus, Bosnia-Herzegovina, Turkey, Ukraine, Moldova, FYR Macedonia, Georgia, Armenia, Albania, Azerbaijan, Russia (European part), and 10 sea regions). Transfer coefficients ν are calculated from sensitivity runs of the EMEP model, in each of which emissions from one source region are reduced by 15%:

$$\nu(\boldsymbol{i}, r) = \frac{c_{NOx}^{base}(\boldsymbol{i}) - c_{NOx}^{red}(\boldsymbol{i})}{0.15\, E_{NOx}^{base}(r)} \qquad (2.2)$$

2020 is used as the base year in the source receptor runs, so that E_{NOx}^{base} corresponds to 2020 emissions taken from the TSAP Baseline scenario. A constant δ_{NOx} quantifies the residual pollution emerging from hemispheric background, natural sources and non-linearities in the system:

$$\delta_{NOx}(\boldsymbol{i}) = c_{NOx}^{base}(\boldsymbol{i}) - \sum_{r=1}^{n_r} E_{NOx}^{base}(r) \cdot \nu(\boldsymbol{i}, r) \quad (2.3)$$

For PM, the same formulation applies, with the exception that both primary PM emissions as well as gaseous precursors must be taken into account. Reduction runs were performed for NH_3 ("A"), NO_x ("N"), PPM ("P"), SO_2 ("S"), and VOC ("V") emissions separately. The equivalent to Eq. (2.1) for PM is then

$$c_{PM}(\boldsymbol{i}) = \delta_{PM}(\boldsymbol{i}) + \sum_{r=1}^{n_r} \sum_{p \in \{A,N,P,S,V\}} E(r,p) \cdot \pi(\boldsymbol{i}, r, p) \quad (2.4)$$

Here, the respective PM transfer coefficient $\pi(\boldsymbol{i}, r, p)$ is dependent on the pollutant, and the sum is taken over all pollutants p in addition to all regions r. The GAINS model distinguishes fine (PM2.5) and coarse (PM2.5-10) PM emissions. Output from the EMEP model is available for PM2.5 and PM10, and transfer coefficients π and constants δ_{PM} are calculated for PM2.5 and PM10 individually. PMcoarse concentrations may be calculated as differences of PM10 and PM2.5 concentrations.

Concentrations at the 28km EMEP grid resolution are not representative for the urban background. For the downscaling step to the urban background level, we use calculations performed with the CHIMERE Chemistry Transport Model (CTM) (Schmidt et al. 2001; Bessagnet et al. 2008). CHIMERE has been used in numerous studies and has undergone extensive validation against observations (Vautard et al. 2005), although at a coarser resolution than used in this study. CHIMERE includes all relevant gas phase and aerosol chemistry (both inorganic and organic secondary aerosol formation). The CHIMERE grid with a resolution of 0.125° (lon) × 0.0625° (lat) or roughly 7×7km is nested within the EMEP grid, so that 16 CHIMERE grid cells exactly match one EMEP grid cell. The extent of the model domain is shown in Figure 2.4, it covers all major cities in the EU. Here we use a full year run of the CHIMERE model with 2009 meteorology and emissions. The gridding of emissions has been undertaken by INERIS, details are given in Appendix A. Several improvements of the CHIMERE model have been made to provide a better representation of urban conditions. These are described in detail in Appendix B.

The same spatial disaggregation of emissions as used in the CHIMERE model was also used for the EMEP model in the transfer coefficient calculations. A detailed description and validation of the CHIMERE model simulation will be available in a separate report.

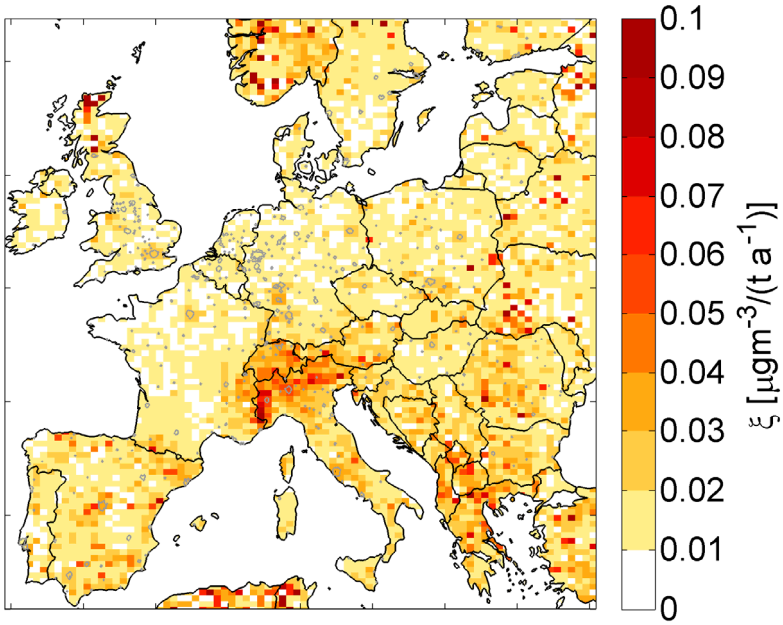

Figure 2.5: NOx downscaling coefficient ξ_{NOx}, i.e. the concentration increase above the EMEP grid average per kt of NOx emitted in a 7km subgrid cell. Negative values of ξ_{NOx}, which exist in low-emission areas, have been set to zero.

As a sensitivity test case, simulations of the EMEP model have been performed at the 7km resolution as well. However, due to the abovementioned urban adjustment measures that have been introduced in the CHIMERE model but not in EMEP, the calculated urban concentration increment is distinctly higher in the CHIMERE output and in better agreement with observations. Therefore, CHIMERE seems more suitable for the downscaling calculations.

The basic concept of the urban increment calculation is the same for NO_x and PM: For each 28km grid cell, we establish a linear relation between deviations of low-level emission densities in the 7km subgrid cells and their corresponding effects in terms of concentration increments in the CHIMERE run. This linear relation is then applied to calculate the urban increment from future emission estimates. A detailed derivation is provided in the following sections for NO_2 (2.3.1) and PM10 (2.3.2) separately.

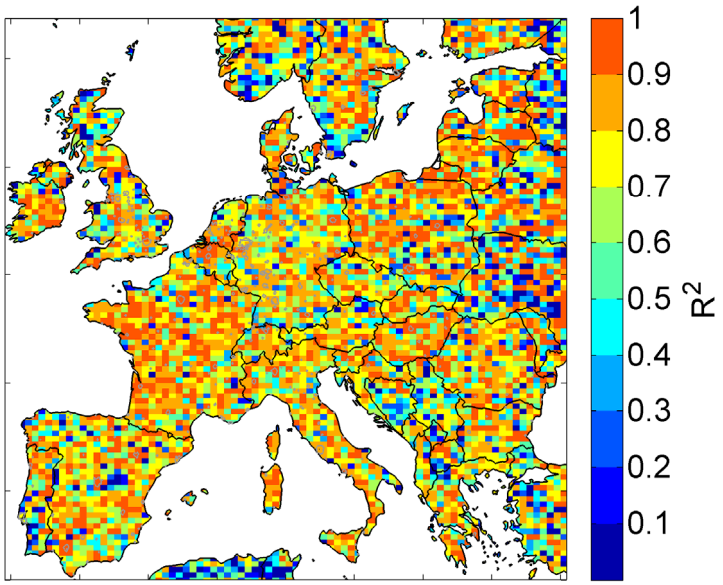

Figure 2.6: Strength of the linear correlation between NOx emissions and concentration increment in the CHIMERE model, expressed as R^2 values.

2.3.1 NO_x and NO_2

Due to the chemical reactivity of NO_2, NO_2 is best treated as a member of the reactive nitrogen NO_x family (NO_x = NO + NO_2). While inter-conversion between NO and NO_2 is fast, their sum NO_x is assumed to be chemically inert within a 28km grid cell: removal of NO_x may happen through the reaction with OH on a timescale of several hours, which is longer than the typical residence time of air in a 28km grid cell. It is thus justified to establish a relation between NO_x emissions and concentrations, while this is not straightforward for NO_2. We calculate NO_x urban background concentrations first, and in a second step derive NO_2 from NO_x by applying the modelled NO_2/NO_x ratio from the respective 7km CHIMERE grid cell. This ratio is left constant for future scenarios, which corresponds to the assumptions that 1) O_3 levels stay constant, and 2) photochemical equilibrium between NO, NO_2 and O_3 is already established at the urban background level. In photochemical steady state, equilibrium concentrations of NO, NO_2 and O_3 are related by

$$\frac{[\mathrm{NO_2}]}{[\mathrm{NO}]} = \frac{k}{J}[\mathrm{O_3}] \qquad (2.5)$$

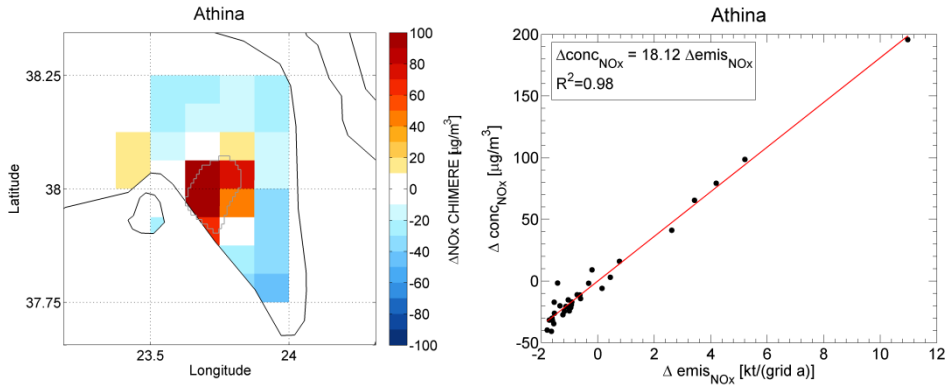

Figure 2.7: Left: NO_x concentration increment around Athens in the CHIMERE model. EMEP grid cells are indicated by thin dotted lines corresponding to axis ticks. Right: Relationship between NO_x low-level emissions and concentration increment around Athens in the CHIMERE model.

with k and J the reaction constants for NO_2 formation and photolysis, respectively (see Section 2.4.1 for a more detailed treatment of NO_2 chemistry).

In the following, the urban increment calculation is derived in detail for the case of NO_x. The explanations apply to PM10 equivalently, so that the discussion of the PM10 increment calculation in Section 2.3.2 is limited to a minimum.

From the CHIMERE model output, a linear relation between low level emissions and the concentration increment within a EMEP grid cell can be established. Let $\boldsymbol{m} = \begin{pmatrix} m_{lon} \\ m_{lat} \end{pmatrix}$ identify a 7km CHIMERE grid and $\boldsymbol{i} = \boldsymbol{i}(\boldsymbol{m}) = \begin{pmatrix} i_{lon}(m_{lon}) \\ i_{lat}(m_{lat}) \end{pmatrix}$ identify the 28km EMEP grid that contains CHIMERE grid $\boldsymbol{m}$. Higher than average NO_x low-level emission density e_{NL} in subgrid $\boldsymbol{m}$ leads to a corresponding increase in ground-level NO_x concentrations above the EMEP grid average, and vice versa for negative deviations. The deviations are related by a regression coefficient ξ_{NOx}, so that

$$\Delta c_{NOx}(\boldsymbol{m}) = \xi_{NOx}(\boldsymbol{i}(\boldsymbol{m})) \cdot \Delta e_{NL}(\boldsymbol{m}) \qquad (2.6)$$

or

$$c_{NOx}(\boldsymbol{m}) = c_{NOx}\big(\boldsymbol{i}(\boldsymbol{m})\big) + \xi_{NOx}\big(\boldsymbol{i}(\boldsymbol{m})\big) \cdot \big\{e_{NL}(\boldsymbol{m}) - e_{NL}\big(\boldsymbol{i}(\boldsymbol{m})\big)\big\} \qquad (2.7)$$

Here $e_{NL}(\boldsymbol{i}(\boldsymbol{m}))$ denotes the average low level emission density in the 28km grid, calculated by averaging the 7km emission densities $e_{NL}(\boldsymbol{m})$ over the respective 28km grid $\boldsymbol{i}$: $e_{NL}\big(\boldsymbol{i}(\boldsymbol{m})\big) = \frac{1}{16}\sum_{\boldsymbol{m}\in\boldsymbol{i}} e_{NL}(\boldsymbol{m}(\boldsymbol{i}))$. Low level emissions contain all sources that are released into the lowest CHIMERE layer: SNAP sectors 2 (domestic), 7 (road traffic), and 8 (non-road traffic). ξ is calculated for every EMEP grid cell $\boldsymbol{i}$ and embeds local meteorological characteristics. EMEP grid cells containing parts of the same urban polygon (see Figure 2.1, detailed explanation below) are combined in the regression to allow for optimal use of information around Europe's major urban areas. A map of ξ values is shown in Figure 2.5. The impact on concentrations of a single ton of pollutant emitted in a grid cell differs

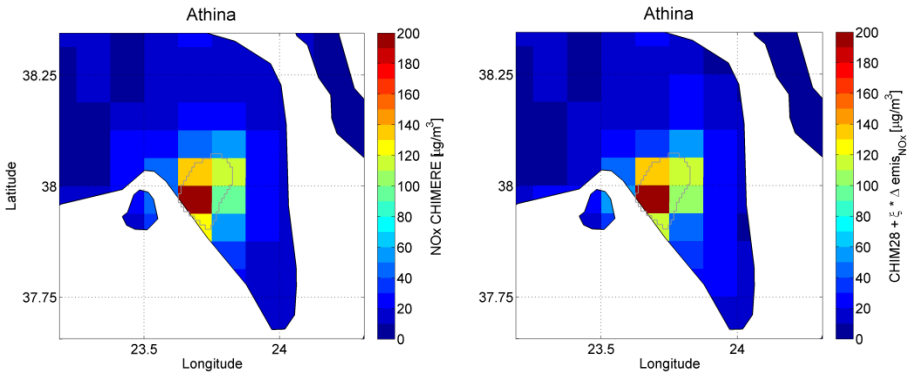

Figure 2.8: NO_x field around Athens in the CHIMERE 7km model run (left), and reconstructed from CHIMERE 28km mean + downscaling using the linear relation between emissions and concentration increment.

significantly with respect to local meteorological conditions – note, e.g., the higher values around the Po valley with frequent stagnant conditions as compared to lower values in Northern Europe. Small negative values of ξ, which do occur randomly in areas with little or no sub-grid emission variability, are filtered out in any further calculation and are not displayed in Figure 2.5. The linear correlation between emissions and concentration increments is quite strong throughout Europe, as shown in Figure 2.6. Particularly in densely populated areas, where both NO_x emission densities and concentration increments are highest, a robust correlation is observed.

Figure 2.7 illustrates the linear relation between low-level emissions and concentration increment for Athens, and Figure 2.8 displays how well the "reconstructed" NO_x concentration pattern matches the original distribution.

The NO_x concentration at the 28km grid level $c_{NOx}(\boldsymbol{i})$ is calculated from transfer coefficients applied to all source regions considered, plus a remaining constant, as described in Eq. (2.1). The downscaling step changes the NO_x concentration in the 7km grid cell $\boldsymbol{m}$ from the EMEP grid average $c_{NOx}(\boldsymbol{i})$ to

$$\mathrm{c_{NOx}(\mathbf{m})} = \sum_{\mathrm{r=1}}^{\mathrm{n_r}} \mathrm{c_{NOx}\,(\mathbf{i}(\mathbf{m}), r)} + \xi(\mathbf{m}) \cdot \left\{ \sum_{\mathrm{r=1}}^{\mathrm{n_r}} \sum_{\mathrm{s=2,7,8}} \mathrm{e_N\,(\mathbf{m}, r, s)} - \sum_{\mathrm{r=1}}^{\mathrm{n_r}} \sum_{\mathrm{s=2,7,8}} \mathrm{e_N\,(\mathbf{i}(\mathbf{m}), s)} \right\} \quad (2.8)$$

$$= \delta_{NOx}(\boldsymbol{i}) + \sum_{r=1}^{n_r} v(\boldsymbol{i}, r) \cdot E_{N,SCEN}\,(r) + \xi(\boldsymbol{m}) \cdot \left\{ \sum_{r=1}^{n_r} \sum_{s=2,7,8} e_{N,CHIM}\,(\boldsymbol{m}, r, s) \cdot \frac{E_{N,SCEN}(r,s)}{E_{N,CHIM}(r,s)} - \sum_{r=1}^{n_r} \sum_{s=2,7,8} e_{N,CHIM}\,(\boldsymbol{i}, r, s) \cdot \frac{E_{N,SCEN}(r,s)}{E_{N,CHIM}(r,s)} \right\} \quad (2.9)$$

Here low-level NO_x emissions have been written as the sum over SNAP sectors 2, 7, and 8 (household, road traffic and non-road traffic emissions). These are the emissions injected into the lowest CHIMERE vertical level, which are assumed to be the main contributors to the urban concentration increment. Gridded NO_x emissions $e_N(\boldsymbol{m}, r, s)$ from source region r and sector s in grid cell $\boldsymbol{m}$ are determined by scaling the gridded emissions used in the CHIMERE run $e_{N,CHIM}(\boldsymbol{m}, r, s)$ with the ratio of scenario vs. CHIMERE national total NO_x emissions from this source region and sector, $E_{N,SCEN}(r,s)/E_{N,CHIM}(r,s)$. Note that gridded emissions (emission densities) are denoted by lowercase e, while capital E is used for national emission numbers.

Practice shows that the concentration enhancement by downscaling to the 7km grid resolution is not sufficient to represent urban background concentrations in many medium-sized and smaller cities, because the 7kmx7km grid is still too large especially if a city is located in more than one grid cell (see schematic illustration in Figure 2.9). Emissions $e_{N,CHIM}(\boldsymbol{m}, r, s)$ (s=2,7,8) do not represent the actual low-level emission density within the urban area but are smeared out over the 7km grid $\boldsymbol{m}$. Hence, to calculate an appropriate concentration increment for the urban part of grid cell $\boldsymbol{m}$, $e_{N,CHIM}(\boldsymbol{m}, r, s)$ needs to be replaced by the higher urban emission density $e^{u}_{N,CHIM}(\boldsymbol{m}, r, s)$. For 376 European cities with a population > 100000, urban polygon shapes have been developed based on population density on a 1km×1km grid. For each city, the urban polygon is designed so that it contains 60% of the city population (shown as red polygons in Figure 2.4, and as red filled polygon in Figure 2.9). Emissions within the polygon $e^{u}_{N,CHIM}(\boldsymbol{m}, r, s)$ are derived from scaling emissions with population density, which is only justified for SNAP2 and SNAP7 non-trucks, while emissions from heavy duty trucks cannot be assumed proportional to population density. For notational convenience, sector SNAP7 truck emissions are labelled 7_T, and SNAP 7 non-truck are labelled 7_n. For sectors 2 and 7_n, the emission density inside these urban polygons is then given by

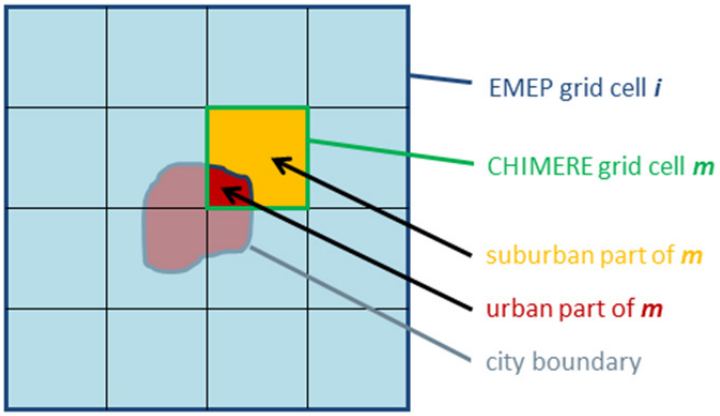

Figure 2.9: Disaggregation of emissions and concentrations in grid cells partly containing urban areas into the urban (red) and suburban (dark yellow) part of the 7km grid cell. The city (red) is distributed over several grid cells, filling only a part of each. To reproduce the concentrations measured by an urban background monitoring station inside the urban area, the higher inner urban emission density is used in the downscaling process.

$$e^{u}_{N,CHIM}(\boldsymbol{m},r,s) = e_{N,CHIM}(\boldsymbol{m},r,p,s)\cdot\frac{pop_u(\boldsymbol{m})}{pop_{tot}(\boldsymbol{m})}\frac{A_{tot}(\boldsymbol{m})}{A_u(\boldsymbol{m})}, \qquad (2.10)$$

pop_u and pop_{tot} representing population and A_u and A_{tot} the area inside the urban polygon vs. the total grid cell. This is effectively a correction of the 7km emission density with the factor $\frac{urban\ population\ share}{urban\ area\ share}$ in grid cell $\boldsymbol{m}$. CHIMERE gridded emissions of sector 7 do not distinguish between trucks and non-trucks; the split is estimated based on national data on truck emission shares. For all other sectors, $e^{u}_{CHIM}(\boldsymbol{m},r,s) = e_{CHIM}(\boldsymbol{m},r,s)$.

Correspondingly, suburban emissions outside the urban polygon in $\boldsymbol{m}$ are lower than the grid cell average. They are given by

$$e^{s}_{N,CHIM}(\boldsymbol{m},r,s) = e_{N,CHIM}(\boldsymbol{m},r,s)\cdot\frac{pop_{tot}(\boldsymbol{m})-pop_u(\boldsymbol{m})}{pop_{tot}(\boldsymbol{m})}\frac{A_{tot}(\boldsymbol{m})}{A_{tot}(\boldsymbol{m})-A_u(\boldsymbol{m})}. \qquad (2.11)$$

Combining all of the above, and using the value for ξ as derived above, we arrive at urban concentrations of NO_x, i.e., concentrations within the part of grid cell $\boldsymbol{m}$ covered by the urban polygon, in the scenario year y,

$$c^{u}_{NOx}(\boldsymbol{m},y) = \delta_{NOx}(\boldsymbol{i}) + \sum_{r=1}^{n_r} v(\boldsymbol{i},r)\cdot E_{N,SCEN}\,(r,y) + \xi_{NOx}(\boldsymbol{m})$$
$$\cdot\left\{\left[\sum_{r=1}^{n_r}\left(\sum_{s=2,7_n,8} e_{N,CHIM}(\boldsymbol{m},r,s)\right.\right.\right.$$
$$\left.\cdot\frac{pop_u(\boldsymbol{m})}{pop_{tot}(\boldsymbol{m})}\frac{A_{tot}(\boldsymbol{m})}{A_u(\boldsymbol{m})}\frac{E_{N,SCEN}(r,s,y)}{E_{N,CHIM}(r,s)}\right) \qquad (2.12)$$
$$\left.+\, e_{N,CHIM}(\boldsymbol{m},r,7_T)\frac{E_{N,SCEN}(r,7_T,y)}{E_{N,CHIM}(r,7_T)}\right]$$
$$\left.-\sum_{r=1}^{n_r}\sum_{s=2,7_n,7_T,8} e_{N,CHIM}\,(\boldsymbol{i},r,s)\cdot\frac{E_{N,SCEN}(r,s,y)}{E_{N,CHIM}(r,s)}\right\}.$$

Correspondingly, concentrations outside the urban polygon (suburban part of the grid cell) are calculated as

$$c^{s}_{NOx}(\boldsymbol{m},y)$$
$$= \delta_{NOx}(\boldsymbol{i}) + \sum_{r=1}^{n_r} v(\boldsymbol{i},r)\cdot E_{N,SCEN}\,(r,y) + \xi_{NOx}(\boldsymbol{m})$$
$$\cdot\left\{\left[\sum_{r=1}^{n_r}\left(\sum_{s=2,7_n,8} e_{N,CHIM}(\boldsymbol{m},r,s)\right.\right.\right.$$
$$\left.\cdot\frac{pop_{tot}(\boldsymbol{m})-pop_u(\boldsymbol{m})}{pop_{tot}(\boldsymbol{m})}\frac{A_{tot}(\boldsymbol{m})}{A_{tot}(\boldsymbol{m})-A_u(\boldsymbol{m})}\frac{E_{N,SCEN}(r,s,y)}{E_{N,CHIM}(r,s)}\right) \qquad (2.13)$$
$$\left.+\, e_{N,CHIM}(\boldsymbol{m},r,7_T)\frac{E_{N,SCEN}(r,7_T,y)}{E_{N,CHIM}(r,7_T)}\right]$$
$$\left.-\sum_{r=1}^{n_r}\sum_{s=2,7_n,7_T,8} e_{N,CHIM}\,(\boldsymbol{i},r,s)\cdot\frac{E_{N,SCEN}(r,s,y)}{E_{N,CHIM}(r,s)}\right\}.$$

As mentioned above, NO_2 concentrations are derived from NO_x concentrations by multiplying c_{NOx} with the NO_2/NO_x concentration ratio in CHIMERE,

$$c_{NO2}(\boldsymbol{m},y) = c_{NOx}(\boldsymbol{m},y)\cdot\frac{c_{NO2,CHIM}(\boldsymbol{m})}{c_{NOx,CHIM}(\boldsymbol{m})} \qquad (2.14)$$

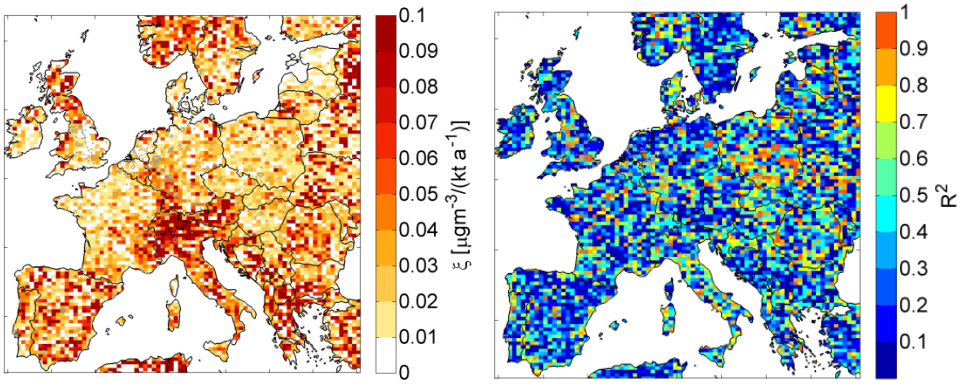

Figure 2.10: Downscaling coefficient ξ and R^2 value of the linear correlation between emissions of primary PM2.5 and PM2.5 concentration increments. Negative values of ξ have been set to zero in the left panel.

2.3.2 PM10

The methodology explained for NO_x in Section 2.3.1 is applied accordingly for PM10 downscaling to the urban background. Only the primary PM field is subject to downscaling, while secondary PM is left unchanged at the 28km resolution as determined from transfer coefficients. Fine and coarse components of PM10 are downscaled independently, by calculating for every EMEP grid cell values of $\xi_{PM2.5}$ and $\xi_{PMcoarse}$. This method takes into account the different aerodynamic mixing properties of fine and coarse PM (sedimentation and local re-suspension is more relevant for the coarse fraction), which may lead to different concentration increments for the same mass amount of pollutant emitted.

The corresponding formula for calculation of urban background PM10 is

$$
\begin{aligned}
& c^{u}_{PM10}(\boldsymbol{m}, y) \\
& = \delta_{PM10}(\boldsymbol{i}) + \sum_{p=A,N,P,S,V} \sum_{r=1}^{n_r} \pi(\boldsymbol{i}, p, r) \cdot E_{SCEN}(r, p, y) \\
& + \sum_{p \in \{PPM2.5, PPMcoarse\}} \xi(\boldsymbol{m}, p) \\
& \cdot \left\{ \left[\sum_{r=1}^{n_r} \left(\sum_{s=2,7_n,8} e_{CHIM}(\boldsymbol{m}, p, r, s) \right.\right.\right. \\
& \left. \cdot \frac{pop_u(\boldsymbol{m})}{pop_{tot}(\boldsymbol{m})} \frac{A_{tot}(\boldsymbol{m})}{A_u(\boldsymbol{m})} \frac{E_{SCEN}(r, p, s, y)}{E_{CHIM}(r, p, s)} \right) \\
& \left. + e_{CHIM}(\boldsymbol{m}, p, r, 7_H) \frac{E_{SCEN}(r, p, 7_T, y)}{E_{CHIM}(r, p, 7_T)} \right] \\
& \left. - \sum_{r=1}^{n_r} \sum_{s=2,7_n,7_T,8} e_{CHIM}(\boldsymbol{i}, p, r, s) \cdot \frac{E_{SCEN}(r, p, s, y)}{E_{CHIM}(r, p, s)} \right\}
\end{aligned}
\tag{2.15}
$$

Correspondingly, concentrations in the suburban part of grid cell $\boldsymbol{m}$ are calculated as

$$
\begin{aligned}
& c^{S}_{PM10}(\boldsymbol{m}, y) \\
& = \delta_{PM10}(\boldsymbol{i}) + \sum_{p=A,N,P,S,V} \sum_{r=1}^{n_r} \pi(\boldsymbol{i}, p, r) \cdot E_{SCEN}(r, p, y) \\
& + \sum_{p \in \{PPM2.5, PPMcoarse\}} \xi(\boldsymbol{m}, p) \\
& \cdot \left\{ \left[\sum_{r=1}^{n_r} \left(\sum_{s=2,7_n,8} e_{CHIM}(\boldsymbol{m}, p, r, s) \right.\right.\right. \\
& \left. \cdot \frac{pop_{tot}(\boldsymbol{m}) - pop_{u}(\boldsymbol{m})}{pop_{tot}(\boldsymbol{m})} \frac{A_{tot}(\boldsymbol{m})}{A_{tot}(\boldsymbol{m}) - A_{u}(\boldsymbol{m})} \frac{E_{SCEN}(r, p, s, y)}{E_{CHIM}(r, p, s)} \right) \\
& \left. + e_{CHIM}(\boldsymbol{m}, p, r, 7_T) \frac{E_{SCEN}(r, p, 7_T, y)}{E_{CHIM}(r, p, 7_T)} \right] \\
& \left. - \sum_{r=1}^{n_r} \sum_{s=2,7_n,7_T,8} e_{CHIM}(\boldsymbol{i}, p, r, s) \cdot \frac{E_{SCEN}(r, p, s, y)}{E_{CHIM}(r, p, s)} \right\}
\end{aligned}
\tag{2.16}
$$

Downscaling coefficients ξ and the related R^2 values are shown in Figure 2.10 and Figure 2.11 for PM2.5 and PM_{coarse}, respectively. Linear relations between low-level primary PM emissions and PM concentration increments are similarly strong in the CHIMERE model as observed for NO_x around major emission hotspots (i.e. major urban areas), while they are generally lower in the countryside. This particularly applies to PMcoarse, as illustrated in Figure 2.11. The overall pattern of the downscaling coefficient $\xi_{PM2.5}$ is similar to that of NO_x, with higher values in the Alpine regions. For PM_{coarse}, the pattern is too noisy in most Member States to draw conclusions about the spatial distribution; however, values of $\xi_{PMcoarse}$ in major cities are similar to those of $\xi_{PM2.5}$. This is illustrated at the example of Paris in Figure 2.12.

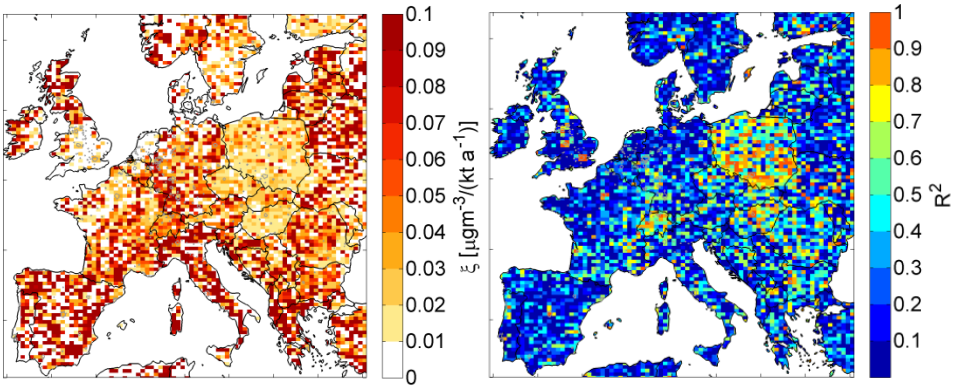

Figure 2.11: Downscaling coefficient ξ and R^2 value of the linear correlation between emissions of primary PM_{coarse} and PM_{coarse} concentration increments. Negative values of ξ have been set to zero in the left panel.

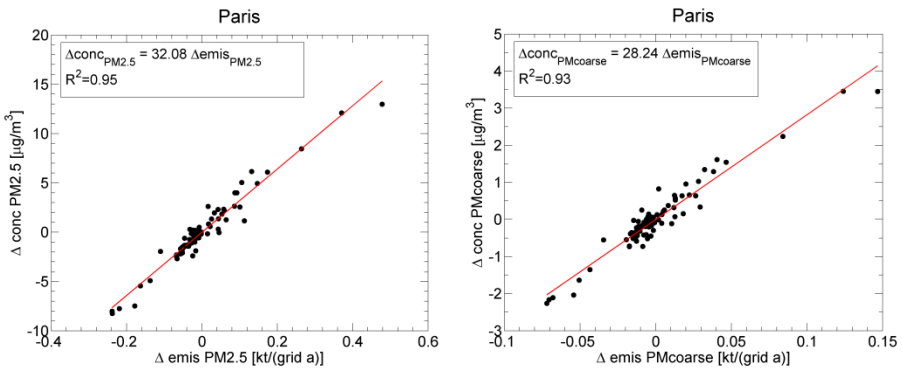

Figure 2.12: Relation between low level PM emissions and concentration increments in Paris, for PM2.5 (left) and PM_{coarse} (right).

2.4 Modelling roadside concentrations

Roadside concentrations of NO_2 and PM10 exceed the respective urban background values significantly at many traffic sites throughout Europe. The concentration difference from urban background to the kerbside is termed traffic increment. Assuming a homogeneous urban background – which is a rather idealized case – the traffic increment is then only a function of the traffic emissions in the particular street.

Modeling of the traffic increment is often done using detailed small-scale chemical dispersion models that take into account local traffic volume, fleet composition, building layout and small-scale meteorology. While these models have provided impressive results for single cities, such bottom-up modeling is not practical for hundreds of traffic stations across Europe, due to lack of data and computing time. Instead, we take a hybrid approach based on the only sources of site-specific information readily available: observations of the relevant pollutants (both at street level and urban background) and station meta data as provided in AirBase.

Downscaling to the urban background was explained in chapter 2.3. The downscaled (7km / inside urban polygon where appropriate) values of PM10 and NO_x provide our best explanation of urban background concentrations originating from anthropogenic emissions. Comparison to measured values shows that - despite a good overall match on average - in many cases a residual fraction remains, in particular for PM10, while in a few cities modeled values exceed measurements.

In our modeling scheme, we adjust modeled background concentrations to match observed values in the base year. Observed background concentrations are obtained as the mean over all AirBase background stations with the same area type (urban, suburban, rural) in the same city if available, or within 20km. If our downscaling scheme under-predicts observations, the offset is regarded as an

unexplained fraction (partly related to sources not contained in the emission inventory, possibly non-anthropogenic, and partly to model imperfections), and is kept constant for future scenarios, since it is impossible to make predictions about the evolution of these sources. On the other hand, an over-prediction of the model is more likely to be related to shortcomings of the simple modeling scheme; in this case, the offset is corrected by a constant (multiplicative) factor. While such a distinction may seem artificial, it ensures that our estimates of future background concentrations are conservative.

The traffic increment itself is then derived as the difference between observed roadside concentrations and the observed background. We employ a simple box model (containing NO_x chemistry for NO_2 stations, and only passive dispersion of fine and coarse particles for PM10 stations) to first explain the observed increment for the base year, and then apply the same box model to future (or past) scenario emissions to model the roadside increment for any scenario year. Modelling of the traffic increment is explained in the following sections for NO_2 (Section 2.4.1) and PM10 (Section 2.4.2) separately.

2.4.1 NO_2

To explain the NO_2 traffic increment, we employ a simple parameterized chemistry model. It calculates roadside NO_2 concentrations from roadside total NO_x (= NO + NO_2) concentrations, urban background NO_2, NO_x, and O_3 concentrations, the fraction of NO_2 in NO_x road traffic emissions, and the residence time of air in the street canyon. This calculation requires roadside concentrations of total NO_x as an input, which can be estimated from past observations and the predicted evolution of emissions.

The unknown residence time of air in the street canyon at a particular monitoring site is determined from AirBase observations, applying the same modeling scheme. To maximize the use of observed information, parameters are estimated for the annual average weekly pattern, which captures the characteristic fingerprint of a traffic station. The annual average weekly pattern contains the largest amount of information that may be extracted from measurements while averaging out effects of highly variable small-scale meteorology that dominate the time series itself. Hence, we use the weekly pattern of NO_2 concentrations with hourly resolution to estimate a set of parameters characterizing each station.

With the site-specific parameters estimated from the weekly cycle of past observations, analysis of emission scenarios is performed using the same chemistry model but with annual average values. Local roadside NO_x concentrations are calculated from scaling the observed NO_x traffic increment with the estimated trend in NO_x road traffic emissions. As a result, estimated roadside concentrations of NO_2 are derived for each scenario year at every road traffic site with sufficient input data (currently 67% of all traffic stations exceeding the annual mean NO_2 limit value).

Chemistry

Besides being emitted directly from vehicles, NO_2 is generated from oxidation of NO and destroyed by photolysis. Typical residence times of air parcels in the immediate surroundings of the road ("street canyon"[4]) before mixing with background air range from seconds to minutes, depending on the layout of the specific street situation (building heights vs. street dimension, average wind speed and direction, etc.), so that only fast chemistry can influence the roadside NO_2 increment. As photochemical equilibrium between NO, NO_2 and O_3 will occur within minutes, NO_x/O_3 chemistry must be taken into account. All other chemistry takes place on longer time scales and thus can be neglected for the sake of simplicity.

We apply a modeling scheme for roadside NO_2 concentrations taking into account direct dispersion of NO_2 emissions, NO_x/O_3 photochemistry, and mixing with urban background. The chemistry scheme itself has been employed before in many applications in NO_2 traffic station modeling (e.g., Düring et al. 2011). Essentially, it is used in the OSPM street pollution model (Berkowicz 2000), and was used in a similar form by Grice et al. (2009) in a Europe wide assessment of roadside NO_2 emissions and concentrations. The NO_x/O_3 photochemistry is represented by

$$\mathrm{NO} + \mathrm{O_3} \xrightarrow{k} \mathrm{NO_2} + \mathrm{O_2} \tag{2.17}$$

$$\mathrm{NO_2} + h\nu \xrightarrow{J} \mathrm{NO} + \mathrm{O} \tag{2.18}$$

$$\mathrm{O} + \mathrm{O_2} + \mathrm{M} \rightarrow \mathrm{O_3} + \mathrm{M} \tag{2.19}$$

In fact, most of the NO_x is emitted as NO, and Eq. (2.17) accounts for a large source of NO_2 in ambient urban air. The fraction of NO_2 in NO_x emissions is denoted as *p*,

$$p = \frac{e_{NO_2}}{e_{NOx}} \tag{2.20}$$

Typical values of *p* are now of the order of 10-20%. They have increased substantially in recent years in countries with a large share of diesel vehicles, and

[4] In the literature, a characterization of street layouts is often made regarding the ratio of street width to building height. In this context, a "street canyon" is usually characterized by a small width/height ratio. Here, we use the term "street canyon" to characterize the immediate surroundings of the roadside monitoring station in question, regardless of its actual layout.

are expected to increase further in the future (see Figure 2.15, and also Grice et al. 2009).

The model assumes that the roadside station, for which NO_2 should be predicted, is coupled to the urban background (i.e., above roof level) through a persistent exchange of air. NO_x is emitted from passing vehicles and accumulates in the street canyon, and is diluted by mixing with background air; at the same time, ozone-depleted air is mixed out and ozone-rich air is mixed into the street, allowing for sustained oxidation of NO. In this simplified system, the urban background serves as a chemical reservoir and is not influenced by emissions in the street under consideration. In the model the mixing process is parameterized by a single time constant τ, so that after a time τ the initial concentration difference between traffic station and urban background has decreased by a factor 1/e, provided that no new emissions occur. Differentially, this can be written as

$$\frac{d}{dt}\left([NO_x]-[NO_x]_B\right)=-\frac{1}{\tau}\left([NO_x]-[NO_x]_B\right) \qquad (2.21)$$

where $[NO_x]$ and $[NO_x]_B$ are roadside and background NO_x concentrations, respectively (analogous notation for all other compounds involved). τ can be understood as the average residence time of an air parcel in the street canyon. It is the single most important parameter describing the physical characteristics of a given street. Typical values of τ range from 40s (open stations) to 100s and more (street canyons).

Dilution of NO_x into the urban background is counteracted by new emissions. The chemical rate equations involving emissions and mixing with the background are

$$\frac{d}{dt}[\mathrm{NO_2}]=k[\mathrm{NO}][\mathrm{O_3}]-J[\mathrm{NO_2}]+\frac{[\mathrm{NO_2}]_V}{\tau}+\frac{[\mathrm{NO_2}]_B-[\mathrm{NO_2}]}{\tau} \qquad (2.22)$$

$$\frac{d}{dt}[\mathrm{NO}]=J[\mathrm{NO_2}]-k[\mathrm{NO}][\mathrm{O_3}]+\frac{[\mathrm{NO}]_V}{\tau}+\frac{[\mathrm{NO}]_B-[\mathrm{NO}]}{\tau} \qquad (2.23)$$

$$\frac{d}{dt}[\mathrm{O_3}]=-k[\mathrm{NO}][\mathrm{O_3}]+J[\mathrm{NO_2}]+\frac{[\mathrm{O_3}]_B-[\mathrm{O_3}]}{\tau} \qquad (2.24)$$

The first two terms in (2.22)-(2.24) describe production and loss of each component through thermal and photochemical reactions (2.17)-(2.19). The last terms in Eqs. (2.22) - (2.24) describe mixing, as in Eq. (2.21), while the second-to-last terms in (2.22) and (2.23) account for the effects of direct NO and NO_2 emissions by vehicles:

$$[\mathrm{NO_2}]_V = p\left([\mathrm{NO_x}]-[\mathrm{NO_x}]_\mathrm{B}\right) \quad (2.25)$$

$$[\mathrm{NO}]_V = \left([\mathrm{NO}]-[\mathrm{NO}]_\mathrm{B}\right) \quad (2.26)$$

Naturally, there is no such term in Eq. (2.24) due to the absence of direct O_3 emissions.

As stated above, chemical equilibrium is attained fast, i.e., all production and loss terms in Eqs. (2.22)-(2.24) cancel out, and we can describe everything in steady state. Therefore, we set the left hand sides of Eqs. (2.22)-(2.24) identically equal to zero, obtaining three algebraic equations with three unknowns ([NO], $[NO_2]$, $[O_3]$). These may be solved to give the steady state solution for $[NO_2]$,

$$[\mathrm{NO_2}]_{ss} = 0.5\left\{B-\sqrt{B^2-4\left([\mathrm{NO}_x][\mathrm{NO_2}]_O+[\mathrm{NO_2}]_n/(k\tau)\right)}\right\} \quad (2.27)$$

with

$$[\mathrm{NO_2}]_n = [\mathrm{NO_2}]_V + [\mathrm{NO_2}]_B \quad (2.28)$$

$$[\mathrm{NO_2}]_O = [\mathrm{NO_2}]_n + [\mathrm{O_3}]_B \quad (2.29)$$

$$B = [NO_x] + [NO_2]_O + \frac{1}{k}\left(J+\frac{1}{\tau}\right) \quad (2.30)$$

Equation (2.27) is well-known and is used regularly to calculate NO_2 from NO_x, e.g., for every time step in the OSPM dispersion model (Berkowicz 2000). Düring et al. (2011) apply it to annual mean concentrations, using annual average reaction constants. Here it is used for two purposes: First, to explain observed NO_2 levels at traffic stations all over Europe from available NO_x observations, thereby estimating the unknown site-specific parameters of the station, and then to calculate steady state NO_2 under future emission conditions. The first step – estimation of site specific parameter values – is done using the annual average weekly concentration pattern with hourly resolution to exploit the maximum amount of information from the measurements, whereas for the application to scenario calculations only annual mean values of concentrations and reaction constants are used as the weekly pattern is not of interest.

Estimation of model parameters

Equation (2.27) is at the core of the traffic station model. Essentially, it is a partitioning equation that determines the share of NO_2 in roadside NO_x. The following inputs are used:

- $[NO_x]$, the local roadside NO_x concentration,
- $[NO_2]_B$, $[NO_x]_B$, $[O_3]_B$, the city average urban background concentrations of the respective gases,

- p, the share of NO_2 in NO_x emissions,
- τ, the characteristic residence time of air in the street canyon,
- J and k, the reaction constants of NO_2 photolysis and NO_2 formation.

For the parameter estimation step, hourly concentrations of $[NO_x]$, $[NO_x]_B$, $[NO_2]_B$, and $[O_3]_B$ are taken from the AirBase data base and averaged by the hour of the week. We require a minimum annual data coverage of 80% for each of the measurements involved. p is available from GAINS emission estimates (only annual mean values are used, no distinction is made into weekdays and weekend). J and k are taken from the literature. For hourly calculations, we use values given by Seinfeld and Pandis (1998) for k, taking into account the observed daily temperature cycle where available, and the country average annual mean temperature otherwise. For J, observed values from Bohn et al. (2005) are used (clear sky observations for March, multiplied with an empirically determined factor 0.8 to account for cloud cover). To account for different insolation, the diurnal cycle of J measured by Bohn et al. (2005) in Juelich, Germany, is scaled with the cosine of the station latitude as a first approximation. Since no physical street canyon dispersion model is employed, the residence time τ needs to be estimated from observations.

Although it is possible to invert Eq. (2.27) and solve for τ, practice shows that this is not sufficient for a reasonable characterization of a traffic site. Reasonable values for τ range from roughly 40 to 100s, while inversion of Eq. (2.27) in several cases gives values distinctly outside these boundaries or even below zero. It is thus not possible to explain roadside NO_2 concentrations at all hotspot sites across Europe with only the mixing time τ as a single site specific parameter. Besides possible shortcomings of our simple modeling scheme (or measurement errors), an obvious reason for this behavior lies in the fact that other input quantities are not known exactly either: Often corresponding background sites are located far from the chosen traffic site (up to 20km distance are allowed in order to ensure sufficient coverage of stations) and are thus not necessarily fully representative of the local background. Thus, even though they are derived from observations, we cannot treat $[NO_2]_B$, $[NO_x]_B$, $[O_3]_B$ as known exactly, but rather as distributions with assumed uncertainty ranges. Owing to the relative positioning of background and traffic stations, a background representativeness correction may be necessary. The three uncertain inputs are rewritten as functions of three dimensionless parameters with certain distributions,

$$[\mathrm{NO_2}]_B = \langle [\mathrm{NO_2}]_B \rangle \cdot \left(1 + \lambda_1 \sigma_{NO_2}\right) \quad (2.31)$$

$$[\mathrm{NO_x}]_B = \langle [\mathrm{NO_x}]_B \rangle \cdot \left(1 + \lambda_1 \sigma_{NO_x}\right) \quad (2.32)$$

$$[\mathrm{O_3}]_B = \langle [\mathrm{O_3}]_B \rangle \cdot \left(1 + \lambda_2 \sigma_{O_3}\right) \quad (2.33)$$

$$\tau = \langle \tau \rangle \cdot \exp(\lambda_3 \sigma_\tau) \quad (2.34)$$

Here $\langle x \rangle$ denotes the expectation value (i.e., the measured value) of quantity x, and σ_x denotes the relative uncertainty of x. λ_1, λ_2, λ_3 are assumed as standard normally distributed (mean = 0, variance = 1). For consistency between the $[NO_2]_B$ and $[NO_x]_B$ adjustments, the same parameter λ_1 is used for both. For calculations with future emission scenarios in which the mean level $\langle x \rangle$ may change substantially, a formulation with relative errors is preferred over additive errors. Uncertainties in the observed background pollutant concentrations due to spatial variability are derived from observations in cities with more than two background measurement stations (10 – 15 cities in Europe are available for each pollutant), with an average standard deviation between 15 – 25%, depending on the pollutant.

The expectation value of τ is set to 70s and the width of the distribution to 30s, in accordance with the literature.

A Monte Carlo based estimation is employed to derive optimal parameter values from the a priori distributions. The aim of this process is to determine values for the input parameters that deviate as little as possible from their a priori expected values, while matching the NO_2 observations as closely as possible. For this purpose, a large sample (N > 100000) of λs is randomly drawn from their distributions, steady state $[NO_2]_{ss}$ is calculated for each combination of λs from Eq. 11, and the optimal subsample is determined by minimizing a penalty function f that weighs the departure of parameters from their a priori expectation values against the offset of $[NO_2]_{ss}$ from observed $[NO_2]_{obs}$, summed up over the whole week:

$$f(n) = \sum_{h=1}^{168} \left(\left|\lambda_{1,n}\right| + \left|\lambda_{2,n}\right| + \left|\lambda_{3,n}\right| + \left| \frac{[NO_2]_{ss}(\lambda_{1,n}, \lambda_{2,n}, \lambda_{3,n}, h) - [NO_2]_{obs}(h)}{\sigma_{obs}} \right| \right) \quad (2.35)$$

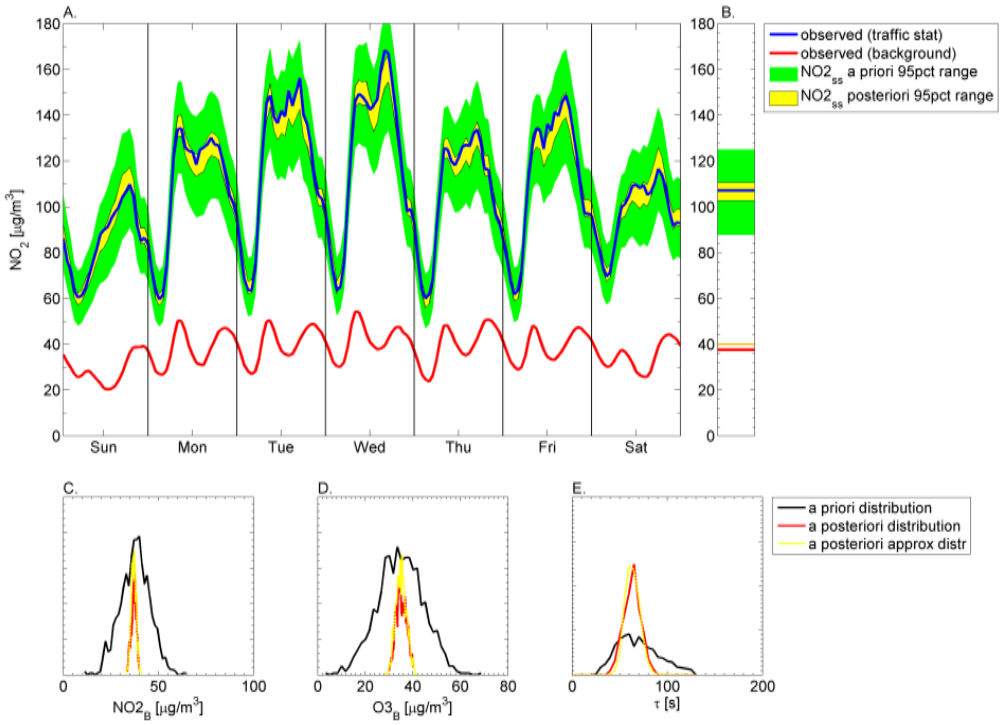

Figure 2.13. Parameter estimation using the observed weekly NO_2 pattern at Marylebone Road station in London. (A): NO_2 traffic station and background weekly pattern, observed and modelled. (B): Average of (A) over the week, corresponding to the annual mean. (C)-(E): Distributions of parameters that enter the model calculations. Week average a priori distributions are shown as black lines, resulting in the green shaded area in the weekly pattern shown in (A) and (B). Tuning leads to the optimized a posterior distributions (red), which are well approximated by Gaussians (yellow dotted). Distributions in (C)-(E) are not normalised. The posteriori parameter distributions result in the posterior NO_2 distribution which is shown as yellow shaded area in (A) and (B).

with n as the index running across the whole sample of N random draws, $n = 1 \ldots N$, $\lambda_{l,n}$ the realization of λ_l in the n^{th} draw, and h the index of the hour of the week. σ_{obs} represents the uncertainty of the roadside [NO_2] observations and is used to determine how strongly the observations must be matched (i.e., to reflect the representativeness of the chosen background station). A too high value of σ_{obs} leads to insufficient matching, while a too small value may lead to over-tuning and unrealistic parameter values. A value of σ_{obs} =0.01 $[NO_2]_{obs}$ was found empirically to provide good results.

The a posteriori distributions of λ_1, λ_2, λ_3, made up from the optimal 1% of parameter combinations minimizing f, are determined and their mean and standard deviation stored for each traffic station considered. The exact form of the penalty function f or the selection criterion is rather arbitrary and may be chosen differently if desired in the future; however, with f as in Eq. (2.35) the tuning process leads to robust solutions for all stations tested so far.

An example for the tuning process is shown in Figure 2.13 for a traffic station in London, UK. The weekly pattern of observations, shown in blue in A and B, is situated well inside the 95% margins of the a priori distribution of $[NO_2]_{ss}$ (green). Minimizing the penalty function (2.35) then narrows down the a priori distributions of input parameters λ_1 … λ_3 to their optimal distributions, leading to the yellow a posteriori (tuned) NO_2 distribution. A priori and a posteriori distributions of the input variables are shown in C – E. The posteriori distributions found by minimizing f (red lines) are very accurately approximated as Gaussians (yellow dotted lines), leaving only two quantities to be stored for each parameter (presently, only the mean is used further).

Application to scenario analysis

To calculate roadside concentrations for future emission scenarios, the urban background values of NO_x and NO_2 are estimated as described in Chapter 2.3, with deviations between observations and modeled concentrations accounted for. Urban background O_3 is left unchanged at the observed levels in the base year, since urban titration effects of NO_x emissions on O_3 are not yet included in the urban background module. The site-specific parameter values (mixing time τ, background representativeness corrections) are derived from the estimation step described above. Although distributions of the parameters are calculated in the tuning process, at this stage of the analysis only the expectation values are used. Since the focus in scenario analysis is not on the weekly pattern of concentrations but on annual mean values, we apply Eq. (2.27) to annual mean concentrations. Here, the daily cycles of reaction constants k and J are replaced by their averages. Results of this annual mean formula are in complete agreement with the mean of weekly pattern concentrations for most stations; only at a few places – typically at stations with severe exceedances of the limit value – the annual mean model tends to give slightly higher concentrations than the average of the weekly cycle with the same parameters.

For estimating roadside NO_x concentrations for future emission scenarios, we consider NO_x as chemically inert at the timescales involved, implying that the NO_x traffic increment is directly proportional to NO_x emissions within the street canyon. The roadside annual mean $[NO_x]$ in a future year y is thus calculated by scaling the NO_x increment observed in the base year y_0 with the expected trend in road traffic emissions E_{NOx},

$$[\mathrm{NO}_x](y) = [\mathrm{NO}_x]_B(y) + \frac{E_{NOx}(y)}{E_{NOx}(y_0)} \cdot \left\{[\mathrm{NO}_x](y_0) - [\mathrm{NO}_x]_B(y_0)\right\}. \qquad (2.36)$$

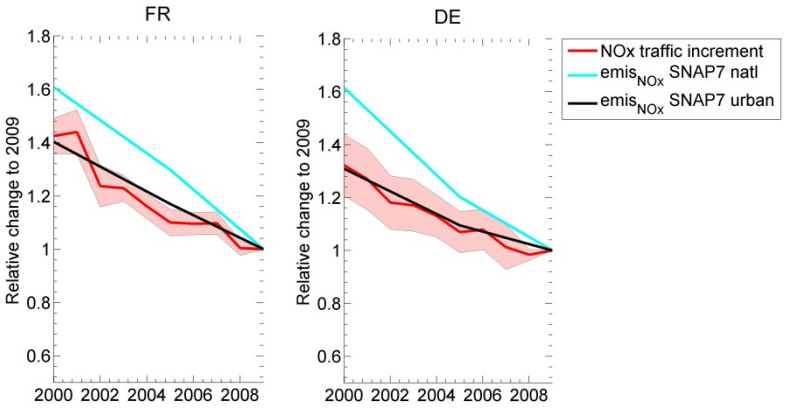

Figure 2.14: Evolution of observed NO_x roadside concentration increment compared the evolution of traffic emissions, normalized to 2009. Red line: mean traffic increment, averaged over all stations; red shaded area: standard deviation of the mean. Blue line: national road traffic emissions, black line: urban road traffic emissions. Emission scenario: TSAP CLE (Dec 2012).

Eq. (2.36) implies that although knowledge of the absolute amount of emissions in the immediate surroundings of the traffic stations is not required, a good estimate of their trend is crucial.

To address this point, we have put considerable emphasis on an improved modeling of traffic emissions under urban driving conditions. To accurately model pollutant emissions from road vehicles it is necessary to determine the vehicle activity, the fleet mix, their age distribution, and their unit emissions under representative driving conditions. The GAINS model has data on all these elements implemented as national averages. Considerable adjustments have been made to derive more representative estimates for urban fleets.

Vehicle fleets are known to differ in composition in urban areas from national average (Carslaw et al. 2011b; Duennebeil et al. 2011; Duering and Baechlin 2009): Notably the share in heavy trucks is much lower in urban driving than on national average, yet there are more buses and motorized two-wheelers. Furthermore the share of diesel cars may differ from the national average. To account for these general differences we determined for each vehicle category its share of miles driven in urban areas. These values are national averages and taken from COPERT (Ntziachristos et al. 2009)(Ntziachristos et al. 2008)(Ntziachristos et al. 2008)Ntziachristos et al., 2008Ntziachristos et al. 2008 or national traffic data (Carslaw et al. 2011a; Knoerr et al. 2011). This way we adjust for the average urban fleet composition in each country.

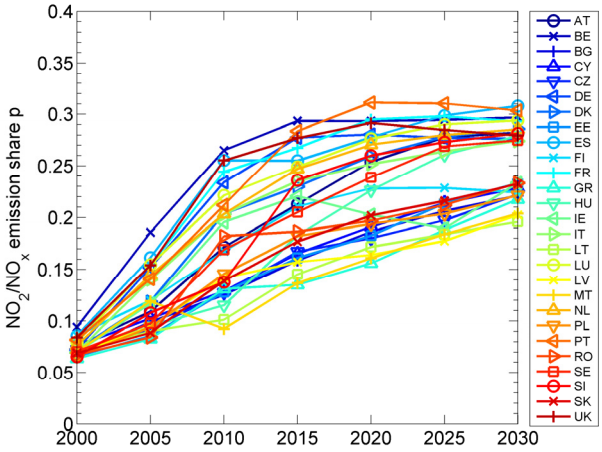

Figure 2.15: Evolution of NO_2 emission share in total NO_x emissions from road transport in the EU27 Member States, as calculated for urban driving conditions under the CLE scenario.

Driving conditions and hence unit emissions differ in urban driving from national average: Speeds are lower, dense traffic and stop-and-go is more frequent, and cold start effects and abrasion from brakes (for PM emissions) play a bigger role than on national average. In particular for heavy duty vehicles it is known that NO_x exhaust after-treatment has not functioned well at urban speeds, and hence unit emissions are several times higher than, e.g., on highway driving. We account for these differences by emissions factors derived explicitly for typical urban driving conditions (on national average) for each country, vehicle category and technology taken from COPERT (Ntziachristos et al. 2009).

Figure 2.14 shows for Germany and France a comparison between the trends in observed NO_x roadside increments (red), averaged over all traffic stations in the country, and NO_x road traffic emission trends in the same country, both for national (blue) and urban (black) driving conditions. All trends are shown normalized to the base year 2009. The mean observed trend in concentration increment is matched very well by the estimated trend in urban driving emissions, while the national traffic emission trend is distinctly different. This clearly demonstrates the need to include the corrections for urban driving as described above.

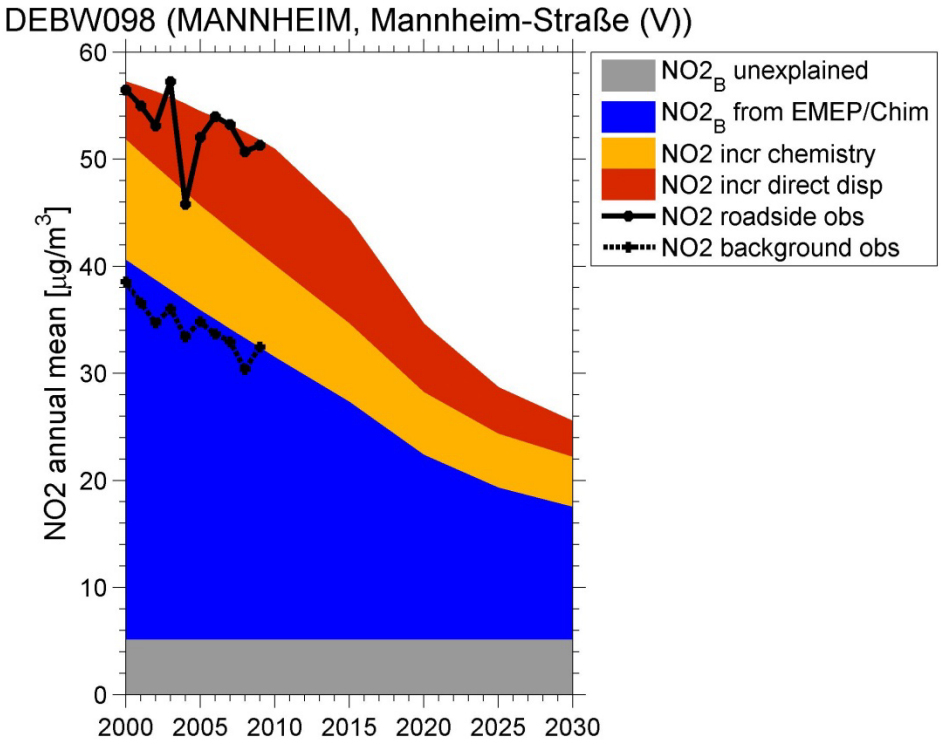

Figure 2.16: Calculated evolution of NO_2 annual mean concentration at a traffic station in Mannheim, Germany, under the TSAP CLE (Dec 2012) scenario, split up into the different components analysed: modelled urban background (blue), unexplained offset to observed urban background (gray), modelled roadside increment from direct dispersion of NO_2 emissions (red), and modelled roadside increment from oxidation of NO emissions (dark yellow). Roadside and urban background observations are shown as solid and dotted lines, respectively.

Also visible in Figure 2.14 is the considerable spread in observed NO_x increment trends at individual monitoring stations, indicated by the red shaded area (standard deviation of the mean). This is due to differences in parameters (fleet composition, driving conditions) that are encountered between different cities, but even between individual roads within the same city. Again, we emphasize that the development of site-specific scenarios for hundreds of traffic stations in the EU is beyond the scope of this project. In the absence of site-specific emission projections, we assume in the GAINS calculations that future traffic emissions at each site will follow the national trend of SNAP sector 7 adjusted for urban driving conditions.

Along with NO_x emissions, also country-specific shares of NO_2 emissions are calculated in GAINS for urban driving situations. Numbers are shown in Figure 2.15 for the current legislation (CLE) scenario. NO_2 emission shares have strongly increased in the past and are expected to continue in the future, mainly due to increasing NO_2 emissions from diesel cars. Consequently, the large spread between different countries reflects the different share of diesel vehicles in the fleet.

Combining all of the above, we calculate annual mean concentrations for future emission scenarios for all traffic stations with sufficient observation data in 2009. As an example, Figure 2.14 shows annual mean NO2 concentrations for a station in Mannheim, Germany, based on observations in 2009 and estimated up to 2030 for the 'current legislation' scenario presented by Amann et al. (2012a). Modelled results are shown as area wedges, disaggregated into urban background (blue), roadside increment from direct dispersion of NO_2 emissions (red), and roadside increment from oxidation of NO emissions (dark yellow). For comparison, observed roadside (solid black line) and urban background (dotted black line) values are shown. From the construction of our model, agreement between observations and modelled values is forced in the base year 2009. Observed values prior to 2009 do not enter the calculations, but are reproduced very well by the model, both for the urban background as well as the traffic station. During the 2000-2009 period, a remarkable shift between the two contributions to the roadside increment are visible: Due to the overall reductions in NO_x (in particular NO) emissions, the magnitude of the chemical increment resulting from NO oxidation decreased, while the direct dispersion of NO_2 gained importance owing to increasing shares of NO_2 in NO_x emissions.

The traffic station depicted in Figure 2.16 shows an excellent match between observations and model results in the 2000-2009 period. However, as many of the site-specific input data for the calculations are subject to natural variability (e.g., annual meteorological conditions) or uncertain (e.g., future traffic volumes and fleet composition in the street canyon, construction activities next to the monitoring site, etc.), predictions for specific sites need to be interpreted with care. More robust conclusions about future compliance with air quality limit values at the large scale can be derived from statistical analyses of a large number of stations where local variability in individual factors are assumed to compensate each other. This approach is discussed further in Chapter 4.2.

2.4.2 PM10

PM10 consists of solid particles with an aerodynamic diameter smaller than 10µm. A distinction is usually made between the fine fraction of PM10 with an aerodynamic diameter < 2.5µm, PM2.5, and the remainder, PM_{coarse}, so that PM10 = PM2.5 + PM_{coarse}. Particles are either directly emitted (primary PM) or formed from gaseous precursors (secondary PM).

The formation of secondary PM takes place on longer time scales, so that within street canyons directly emitted particles make the larger contributions to the observed road side increment. While similarities exist between the dispersion of PM and chemically inert gases, in contrast to gaseous substances, PM can accumulate on the surface as dust which may later be re-suspended by air motion.

Traffic-related sources of PM10 include not only direct exhaust emissions, but also tire and break wear and road abrasion. While exhaust emissions are well quantified and have been regulated, there are large uncertainties regarding the magnitude of non-exhaust emissions (Boulter 2005). In spite of these uncertainties and inconsistencies in the literature, however, the importance of non-exhaust emission sources has repeatedly been emphasized, in particular for the coarse fraction of PM with an aerodynamic diameter > 2.5µm (Amato et al. 2009; Thorpe and Harrison 2008; Kupiainen et al. 2005). PM_{coarse} has been found to consist almost entirely of non-exhaust particles (Harrison et al. 2012), and at the same time is more affected by resuspension as it may accumulate on the road surface. Between different regions, large differences exist in the size partitioning and thus exhaust or non-exhaust origin of the PM10 roadside increment: in London, Harrison et al. (2001) determined a roughly even split of the roadside increment in PM2.5 and PM_{coarse}, largely consistent with many continental European sites (see e.g. Figure 2.18), while in Nordic countries the coarse fraction dominates, caused by the widespread use of studded tires and application of traction sanding in winter (Kupiainen et al. 2005; Omstedt et al. 2005).

The approach followed here distinguishes and idealizes the fine and coarse fractions of PM, assuming that primary PM2.5 is dispersed like a chemically inert gas while PM_{coarse} is subject to accumulation and resuspension. Mathematically, this is expressed by postulating for PM2.5 a relation between emissions and roadside concentration increment in the form of

$$\Delta[\mathrm{PM2.5}] = \alpha \cdot emis_{\mathrm{PM2.5}} \tag{2.37}$$

Thereby, the resulting effect in terms of concentration is directly proportional to the emissions. For PM_{coarse}, on the other hand, the resulting concentration increment may be larger than expected from the dispersion of primary emissions,

$$\Delta[\mathrm{PM}_{coarse}] > \alpha \cdot emis_{\mathrm{PM}coarse} \tag{2.38}$$

and thus also

$$\Delta[\mathrm{PM}_{10}] > \alpha \cdot emis_{\mathrm{PM10}} \tag{2.39}$$

Finding a functional relation between coarse particle emissions and their concentration effects is not straightforward, due to resuspension and sedimentation, which are dynamic processes. The passage of a single vehicle may cause very little or very large emissions, depending on external conditions such as wind direction and speed, road surface humidity and traffic density. In a street canyon, already a few vehicles may be able to entrain much of the available dust, while the additional contribution of a single vehicle on a busy road may be negligible. Consequently, the difficulties in determining emission factors for resuspension have been repeatedly emphasized (Lohmeyer and Duering 2001; Boulter 2005; Amato et al. 2009; Gehrig et al. 2010), and emission factors given by different studies vary by orders of magnitude.

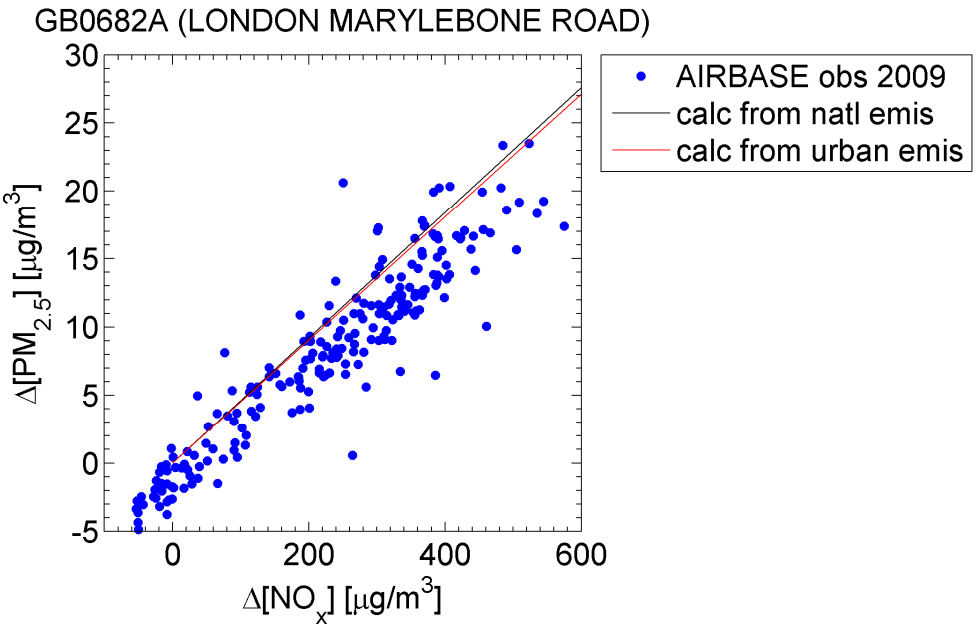

Figure 2.17: PM2.5 vs. NO_x traffic increment measured at Marylebone Road station in London, UK, in 2009 daily AirBase data. Solid lines represent the linear relation given in Eq. (2.40), using either national PM2.5 and NO_x emissions, or emissions under urban driving conditions.

For these reasons we do not attempt to quantify the functional relation between $emis_{PMcoarse}$ and $\Delta[PM_{coarse}]$. Instead, we model the expected fine particular traffic increment Δ[PM2.5] from PM2.5 emissions and interpret the difference to measured Δ[PM10] as the contribution of PM_{coarse} due to primary emissions and resuspension. The expected magnitude of Δ[PM2.5], $\Delta[PM2.5]_{mod}$, is calculated from Eq. 2.37, where α is substituted by the Δconcentration/emission ratio from a chemically inert gas such as NO_x,

$$\Delta[\mathrm{PM2.5}]_{\mathrm{mod}}(t_0) = emis_{\mathrm{PM2.5}}(t_0)\frac{\Delta[\mathrm{NO}_x](t_0)}{emis_{NOx}(t_0)} \qquad (2.40)$$

It should be emphasized that neither PM2.5 nor NO_x emissions need to be known for the street in question, but only their ratio, which may be calculated directly from the emission factors. The proportionality between NO_x and PM increments has repeatedly been reported and used, e.g. by Harrison et al. (2001) and Boulter et al. (2006). Figure 2.17 illustrates this relation for Marylebone Road monitoring station in London, showing that (aside from a small offset) the PM2.5 increment linearly follows the NO_x increment with the proportionality exactly as expected from Eq. (2.40).

Provided that (2.40) gives a reasonable estimate for Δ[PM2.5], the remainder to observed $\Delta[PM10]_{obs}$ in the base year must then be due to PMcoarse,

$$\Delta[\mathrm{PM}_{\mathrm{coarse}}]_{\mathrm{mod}}(t_0) = \Delta[\mathrm{PM10}]_{\mathrm{obs}}(t_0) - \Delta[\mathrm{PM2.5}]_{\mathrm{mod}}(t_0) \qquad (2.41)$$

Thereby the model is forced to reproduce the exact level of observed Δ[PM10] in the base year, except for the very few cases where $\Delta[\mathrm{PM2.5}]_{\mathrm{mod}}$ is already larger than $\Delta[\mathrm{PM10}]_{\mathrm{obs}}$ (in this case, $\Delta[\mathrm{PM}_{\mathrm{coarse}}]_{\mathrm{mod}} = 0$). While this may not be ideal from a modeller's point of view, it circumvents the abovementioned difficulty of establishing a relation between $\mathrm{PM}_{\mathrm{coarse}}$ emissions and their corresponding effect on the concentration increment.

In order to validate this modeling approach, $\Delta[\mathrm{PM2.5}]_{\mathrm{mod}}$ estimated from Eq. (2.40) needs to be compared to observations. Unfortunately, only few AirBase measurement sites provide the necessary combination of roadside and background PM10 and PM2.5 observations. A comparison of modelled and measured values for sites with data for 2009 is shown in Figure 2.18. Generally, the order of magnitude of Δ[PM2.5] is captured well by the model, although a tendency to overestimate is visible. Typically between 1/3 and 2/3 of Δ[PM10] is fine increment; however, uncertainties in the observations are considerable (note, e.g., negative Δ[PM2.5] or reported Δ[PM2.5] exceeding Δ[PM10]!).

For future emission scenarios, $\Delta[\mathrm{PM2.5}]_{\mathrm{mod}}$ and $\Delta[\mathrm{PM}_{\mathrm{coarse}}]_{\mathrm{mod}}$ are modeled for the base year t_0 and scaled with the evolution of emissions at different times (years) t. For Δ[PM2.5], according to Equation (2.38) the concentration increment scales directly proportional to PM2.5 traffic emissions, so that

$$\begin{aligned}\Delta[\mathrm{PM2.5}]_{\mathrm{mod}}(t) &= \frac{emis_{\mathrm{PM2.5}}(t)}{emis_{\mathrm{PM2.5}}(t_0)}\Delta[\mathrm{PM2.5}]_{\mathrm{mod}}(t_0) \\ &= emis_{\mathrm{PM2.5}}(t)\frac{\Delta[\mathrm{NO}_x](t_0)}{emis_{NOx}(t_0)}\end{aligned} \qquad (2.42)$$

The situation is not as clear for the coarse increment. However, it is reasonable to argue that $\Delta[\mathrm{PM}_{\mathrm{coarse}}]$ should scale with the traffic volume. This is confirmed by the observed weekly pattern at the very few sites that supply hourly PM2.5 and PM10 data for a combination of a traffic and corresponding background stations: While the coarse fraction contributes disproportionally much to the concentration increments, it exhibits a clear traffic pattern. This observed traffic pattern in hourly $\Delta[\mathrm{PM}_{\mathrm{coarse}}]$ suggests that it should not be treated as constant in the future, but rather scaled with $\mathrm{PM}_{\mathrm{coarse}}$ road traffic emissions, which originate entirely from non-exhaust sources:

$$\Delta[\mathrm{PM}_{coarse}]_{\mathrm{mod}}(t) = \frac{emis_{\mathrm{PM}coarse}(t)}{emis_{\mathrm{PM}coarse}(t_0)}\Delta[\mathrm{PM}_{coarse}]_{\mathrm{mod}}(t_0) \qquad (2.43)$$

As non-exhaust emission sources (brake and tire wear, road abrasion, road dust re-suspension) are currently not controlled, emissions should develop proportional to traffic volume.

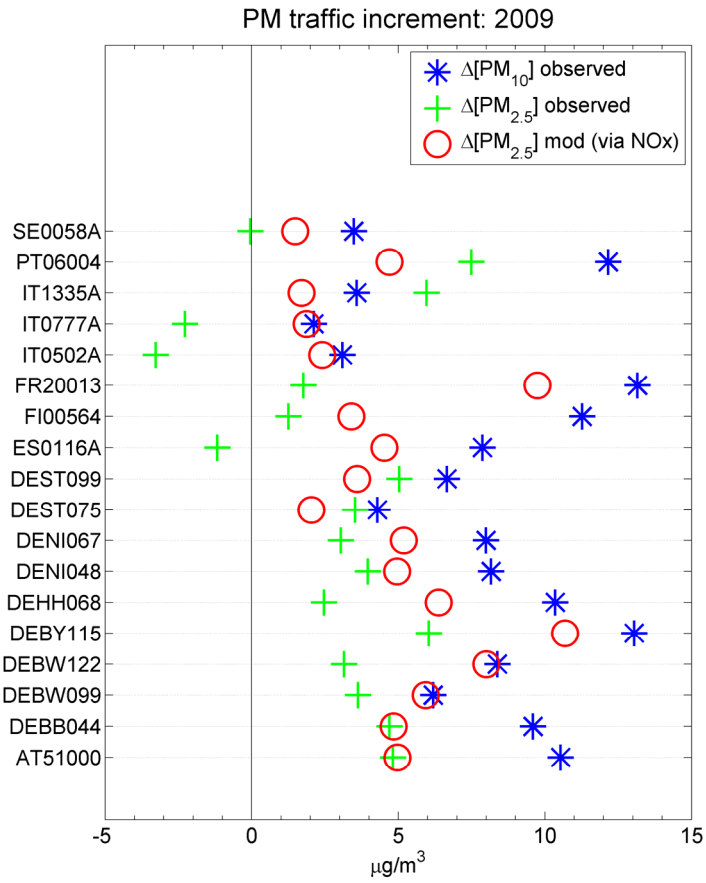

Figure 2.18: Comparison between observed and modeled PM2.5 traffic increment, and their relation to the observed PM10 traffic increment.

Combining (2.42)-(2.43), we arrive at the following expression for the estimated PM_{10} traffic increment at time (year) *t*:

$$\Delta[\mathrm{PM10}]_{\mathrm{mod}}(t) = emis_{\mathrm{PM\,2.5}}(t)\frac{\Delta[\mathrm{NO}_x](t_0)}{emis_{NOx}(t_0)} + \ldots$$
$$\frac{emis_{\mathrm{PMcoarse}}(t)}{emis_{\mathrm{PMcoarse}}(t_0)}\left\{\Delta[\mathrm{PM10}]_{\mathrm{obs}}(t_0) - emis_{\mathrm{PM\,2.5}}(t_0)\frac{\Delta[\mathrm{NO}_x](t_0)}{emis_{NOx}(t_0)}\right\} \quad (2.44)$$

Again, it should be emphasized that with this approach increments at each individual station are expected to follow the national emission trends. Although this assumption is unrealistic, it is still the best possible assumption without detailed knowledge of the traffic situation and site specific evolution in the future. At the same time, if such additional site-specific information becomes available, it will be straightforward to adjust the appropriate emission scenario.

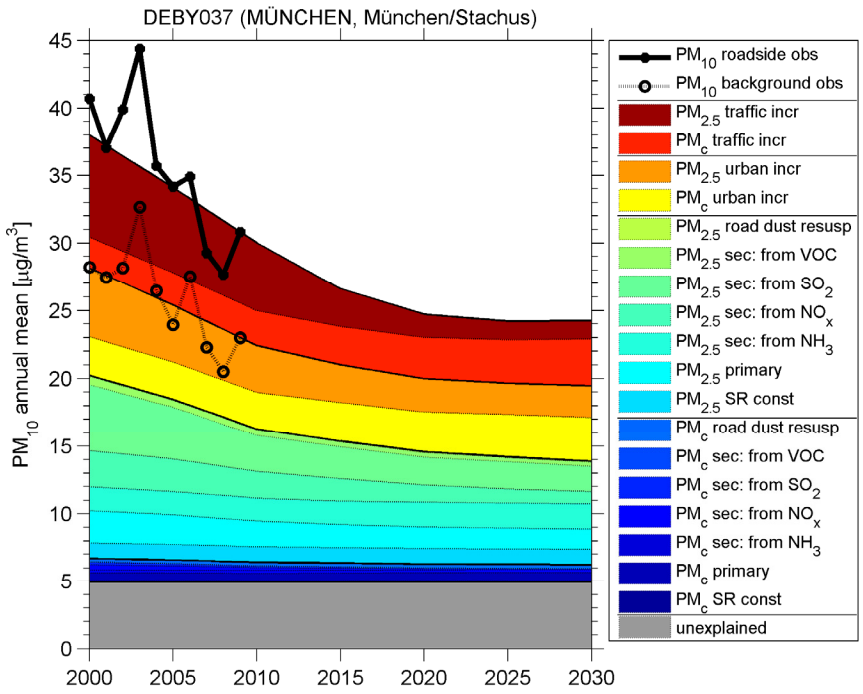

Figure 2.19: Modelled evolution of PM10 at a traffic station in Munich, Germany, disaggregated into the different components considered. For enhanced readability, components are grouped into categories as indicated by segregation lines in the legend and solid black lines in the area plot: unexplained PM10 background, coarse PM background from transfer coefficients (28km grid), PM2.5 background from transfer coefficients (28km grid), PM_{coarse} urban increment, PM2.5 urban increment, PM_{coarse} roadside increment, PM2.5 roadside increment. Emission scenario: TSAP CLE (Dec 2012).

An example of modeled concentrations is shown in Figure 2.19 for a traffic station in Munich, Germany. Here, the split into different components is explicitly shown: PM2.5 and PM_{coarse} background (28km grid), urban increment, and traffic increment, as well as the unexplained part. At the 28km level, contributions are disaggregated into primary and secondary PM. Observed roadside and background concentrations are shown as solid and dotted black lines, respectively. Numerical results should be interpreted with caution, as explained for Figure 2.16 for the case of NO_2. Figure 2.16 and Figure 2.19 display the endpoint of model calculations for each individual traffic station for which sufficient data are available in AirBase.

3 Validation

In this chapter, the urban background and traffic station modules introduced in Chapter 2 are validated against observations. Section 3.1 assesses the quality of the modelled urban background for the base year 2009, while Section 3.2 discusses trends, with a particular focus on the traffic station scheme.

3.1 Urban background

3.1.1 NO_2 and NO_x

Figure 3.1 shows scatter plots of observed versus modelled NO_2 annual mean concentrations at AirBase background stations in the year 2009. Different categories of background stations are indicated by different colours and symbols. For urban background stations, which are most relevant for the downscaling methodology, a distinction is made into cities for which an urban polygon is available, and all others. For cities where urban polygon shapes are available, the downscaled concentration inside the urban polygon is shown as the modelled value (red dots), and the concentration downscaled to the 7km grid otherwise (red circles). While modelled values for cities with urban polygon adjustment generally match observations well, those in cities without urban polygons show a tendency to underestimate. This is explained by the fact that these cities are rather small in size, thus not filling an entire 7km grid cell. For these cities, a redistribution of emissions according to population density might improve results considerably. On the other hand, in major urban areas such as Paris, Barcelona or London, urban background observations are exceeded by the modelled values. This phenomenon is seen in the CTM output as well and may be related to mis-allocation of emissions in cities, or too strong wind speed corrections in the CHIMERE model. In these cases, the urban polygon adjustment does not influence results, since it is effective only in city boundary grid cells partly covered by the urban polygon, while the inner city 7km grid cells with peak concentrations lie completely within the urban polygon.

For suburban background stations, the value outside the urban polygon or (if no urban polygon is defined in the respective grid cell) the 7km grid cell value is taken for comparison here.

The equivalent plot for NO_x is shown in Figure 3.2. The spread is larger for NO_x than for NO_2, indicating that NO_2 is better captured than NO in CHIMERE. This may be related to the smaller spatial variability in ambient NO_2 than total NO_x concentrations.

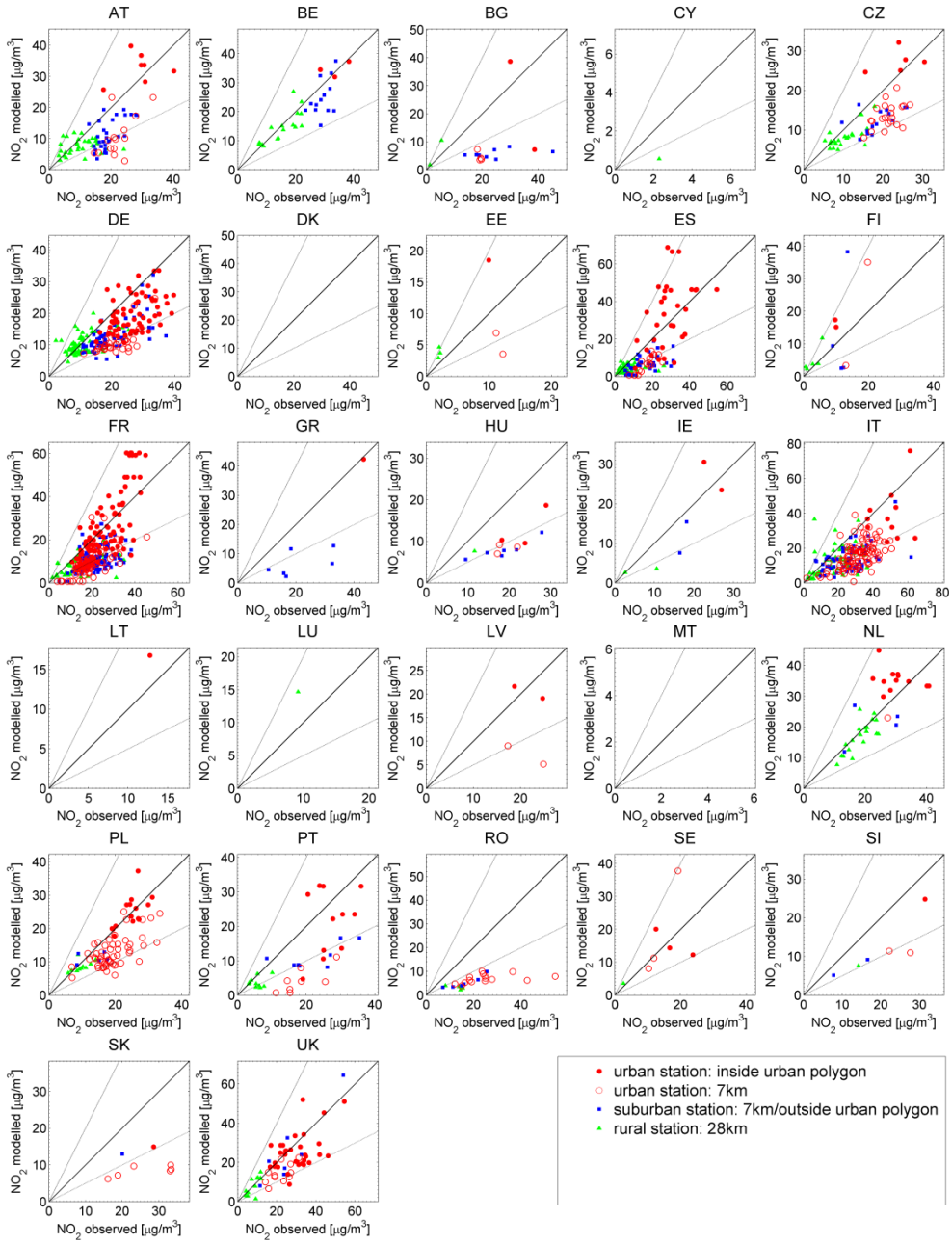

Figure 3.1: NO_2 annual mean concentrations at different categories of AirBase background stations, observed vs. modelled values. Modelled values represent concentrations obtained from transfer coefficients at the 28km resolution (rural stations), downscaled to the 7km grid and outside urban polygons (suburban stations), and inside urban polygons (urban stations, red dots). For those urban stations where no urban polygon information is available, the 7km downscaled value is shown (open red circles).

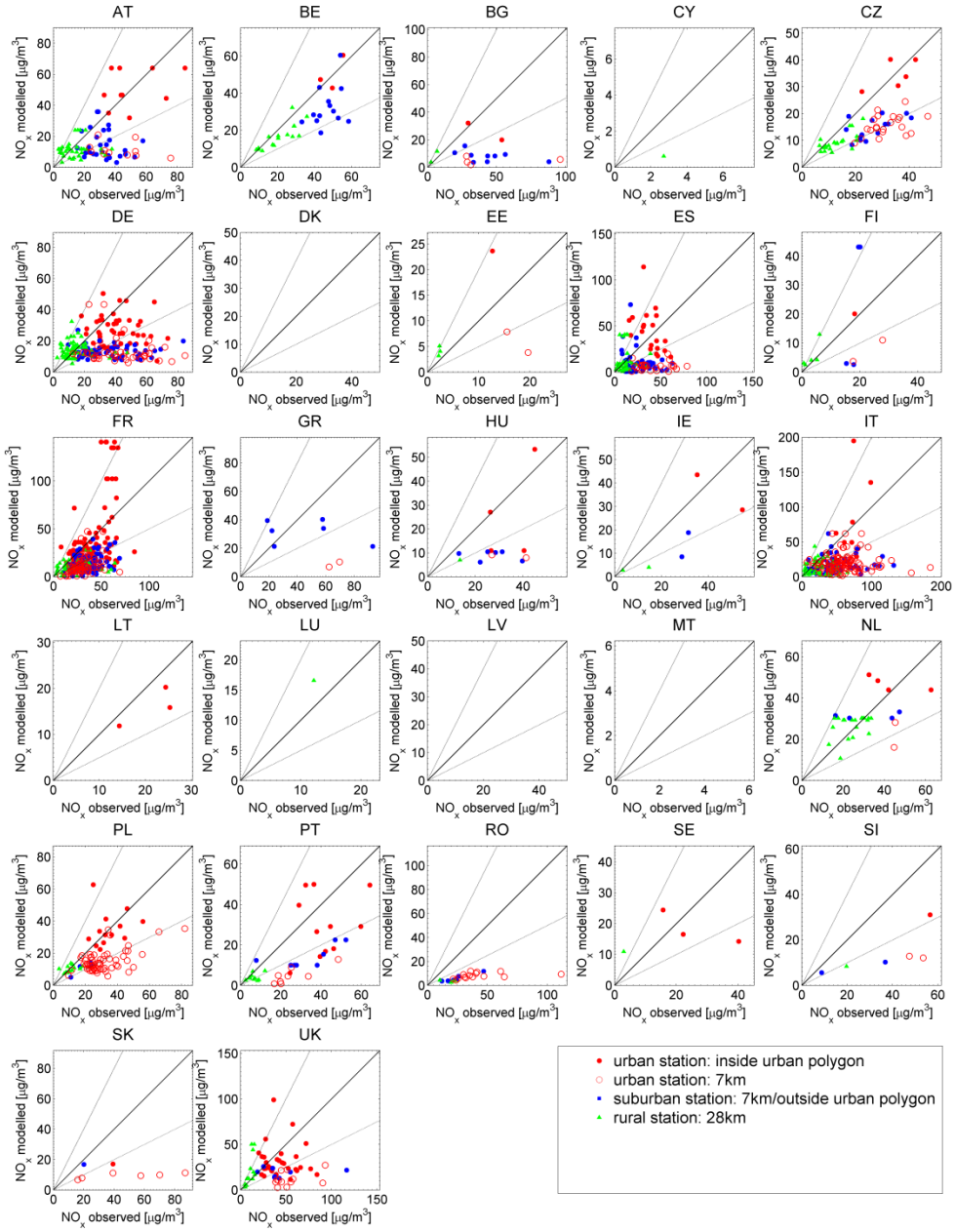

Figure 3.2: As Figure 3.1 but for NO_x.

3.1.2 PM10

As explained in Section 2.3.2, fine and coarse PM are downscaled individually and hence validated separately. Overall we find that modelled PM2.5 is by far in better agreement with observations than PM_{coarse}, which may be related, inter alia, to large uncertainties in PM_{coarse} emission inventories.

Unfortunately, the number of measurement stations providing data for both fine and coarse PM is limited. Figure 3.3 shows the comparison of downscaled PM2.5 values to observations for all available stations in 2009, in the same way as in Figure 3.1. Although the correlation between measurements and modelled results varies between different countries, the order of magnitude is estimated correctly at most stations, and most stations are located well within the factor of two offset margins.

For PM_{coarse} (Figure 3.4), larger discrepancies are observed. Although some countries are modelled quite well (e.g., Portugal), in most countries the spatial variability is strongly underestimated, and high observed values are not reproduced in the model. Possible reasons for this behaviour range from large uncertainties in emission inventories to a very limited representation of dust re-suspension in the model.

Finally, Figure 3.5 shows the comparison for PM10. Note that this is not redundant to the combination of Figure 3.3 and Figure 3.4, as the disaggregation into PM2.5 and PM_{coarse} is only measured at a subset of PM10 stations. The picture from the validation of fine and coarse components is largely confirmed in Figure 3.5: Most stations lie within a factor of two margins around observations. Correlation between observations and model varies between countries, but there is a tendency to under-estimate the spatial variability within countries, so that high measured values are underestimated. From Figure 3.4, we may assume that a large part of the unexplained PM10 background fraction is indeed PM_{coarse}. Since there are no major trends for PM_{coarse} estimated, compensating missing PM10 by a constant offset should not affect the quality of the modelled PM10 urban background trend.

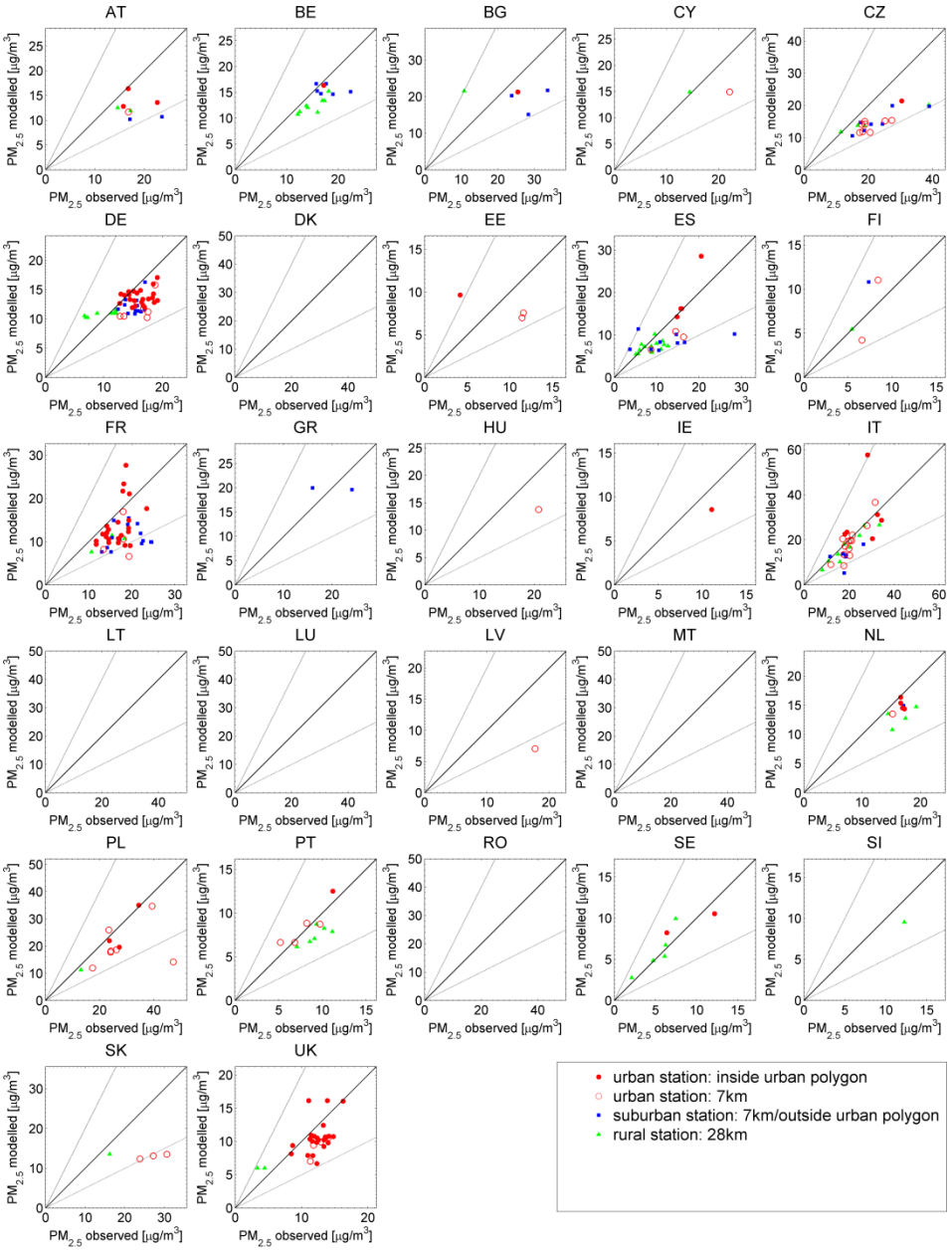

Figure 3.3: As Figure 3.1 but for PM2.5. Dust and sea salt fields as used in the EMEP model (2009 run) have been added to modelled concentrations to make them comparable with observations.

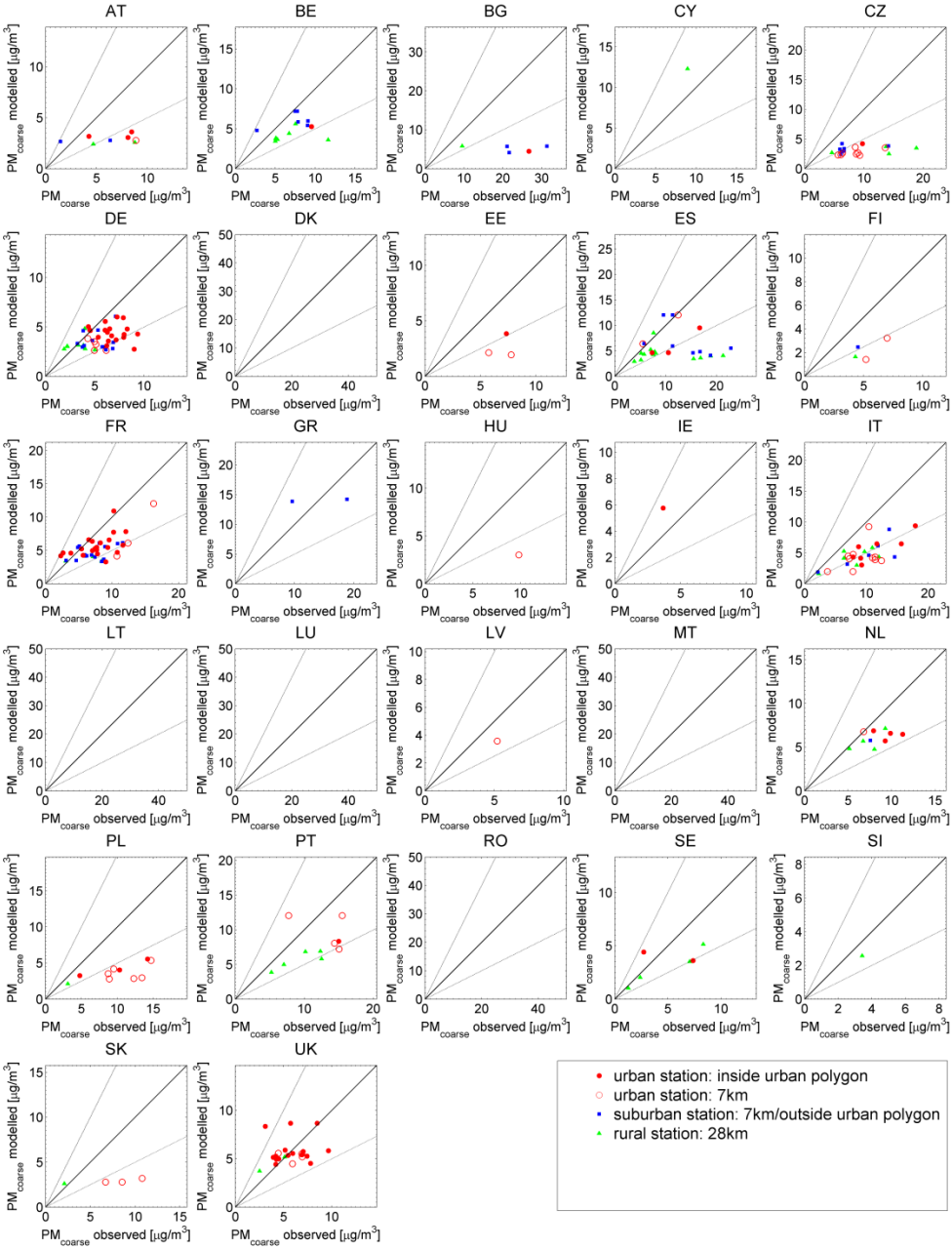

Figure 3.4: As Figure 3.1 but for PM_{coarse} = $PM_{2.5-10}$.

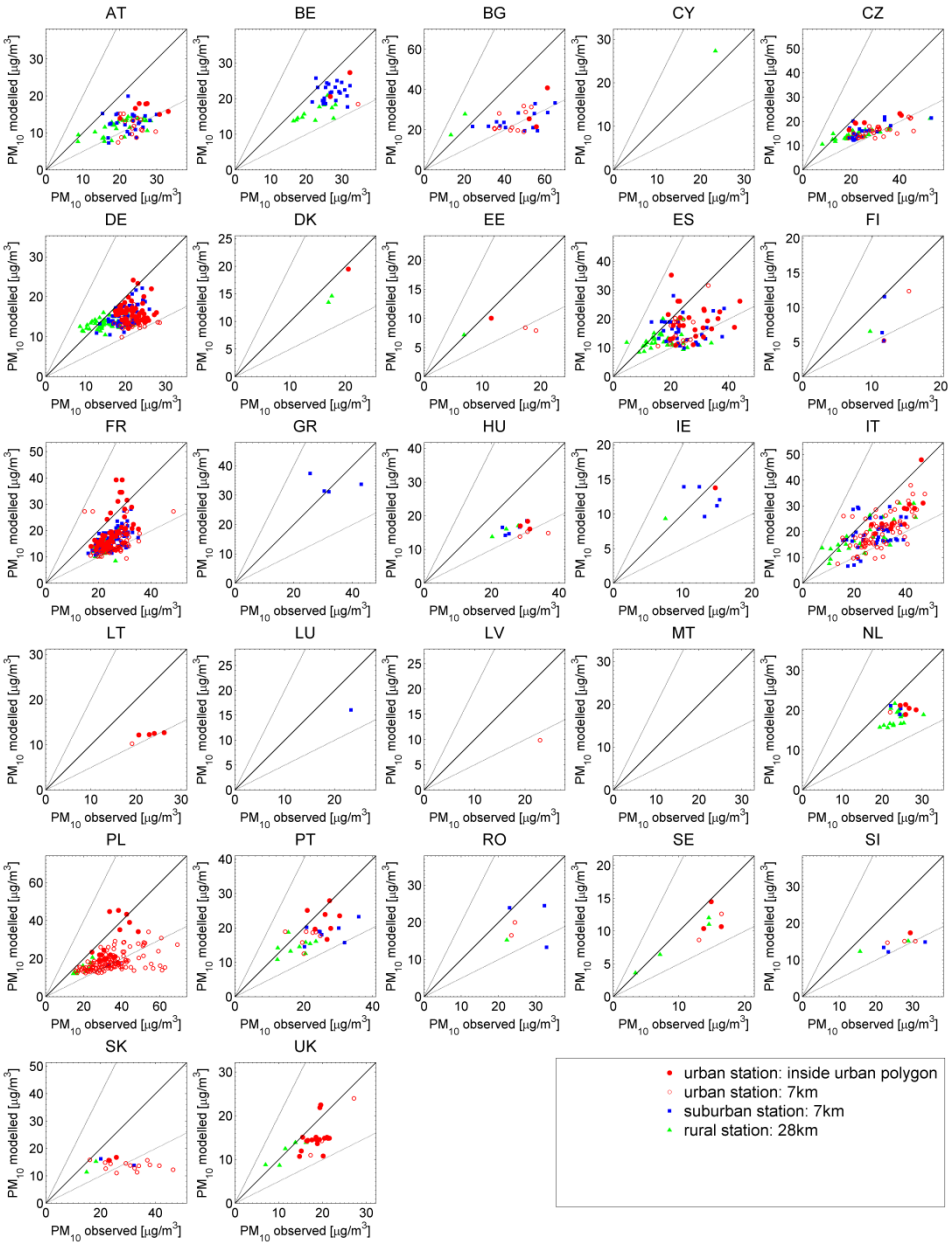

Figure 3.5: As Figure 3.1, but for PM10.

3.2 Roadside concentrations

Modelled concentrations have been calculated for around 2000 AirBase measurement sites across Europe (2020 sites for NO_2, 1902 for PM10 with the present data coverage criteria applied), among them 432 NO_2 and 322 PM10 traffic stations. Although the focus of the station modelling scheme is on traffic stations, exceedances of limit values are not only observed at stations classified as traffic stations, and for the sake of consistency also modelled concentrations at other station categories are included in this section.

From the construction of the station specific modelling scheme, model results are forced to be consistent with observations in the base year. For background stations, this requirement is absolute: differences between observations and downscaled model results from source receptor relations are compensated by a constant offset (in case of model underestimate) or a constant factor (in case of model over-estimate) on a station by station base. For traffic stations, the background concentrations involved are adjusted to match the city average observations. For roadside concentrations, the requirement for consistency between model results and observations in the base year is not as strict: In the case of NO_2, site specific parameters obtained from the weekly pattern may give slightly different results when used for prediction with the annual mean model. In the case of PM10, at a few sites the estimated PM2.5 traffic increment exceeds the observed PM10 increment. In this case no PM_{coarse} traffic increment is calculated, but the resulting overestimation of observed total roadside PM10 is not compensated in the model.

Because of this inherently forced consistency between model and observations in the base year, only a trend validation is reasonable. Model results presented in this section were calculated for the emission years 2000-2009 (emissions interpolated linearly between 2000, 2005, and 2010), using transfer coefficients averaged over five meteorological years and 2009 as the base year for the estimation of site specific parameters.

3.2.1 NO_2

Figure 3.1 shows a comparison of modelled and observed annual mean NO_2 concentrations averaged over the EU27, for different categories of AirBase stations. For each year, the set of stations is restricted individually to those both modelled and operational in the particular year. It is obvious from this figure that for traffic stations even the mean of all European stations clearly exceeds the limit value. Small improvements have been seen in the decade shown here: At all station categories except perhaps the rural background stations, a small downward trend in NO_2 concentrations is observed. For traffic stations, the trend is matched perfectly by the model (for the explanation of the small offset of about 1µg/m^3, see introductory paragraph to Section 3.2 above). At urban, suburban and rural background stations, this trend is slightly overestimated by the model, so that modelled concentrations in the early years exceed observations by a few µg/m^3. To our understanding, the reason for this lies in the assumption of NO_2-NO-O_3 equilibrium, i.e., that urban background NO_2 is not directly influenced by NO_2 emissions and should – in the absence of O_3 changes – follow the NO_x trend. In reality, the strong increases in NO_2 emission shares (see Figure 2.15) have led to the more stagnant NO_2 values seen in Figure 3.6. While this mismatch is annoying, the absolute effects are small (about 2µg/m^3 in 2000). Expected changes of the NO_2 emission share p are somewhat smaller in the future (an expected 50%

increase between 2010 and 2030 as compared to a doubling from 2000 to 2010, see Figure 2.15), so that the assumption of urban background NO_2 as a constant fraction of urban background NO_x should be better fulfilled than in the past.

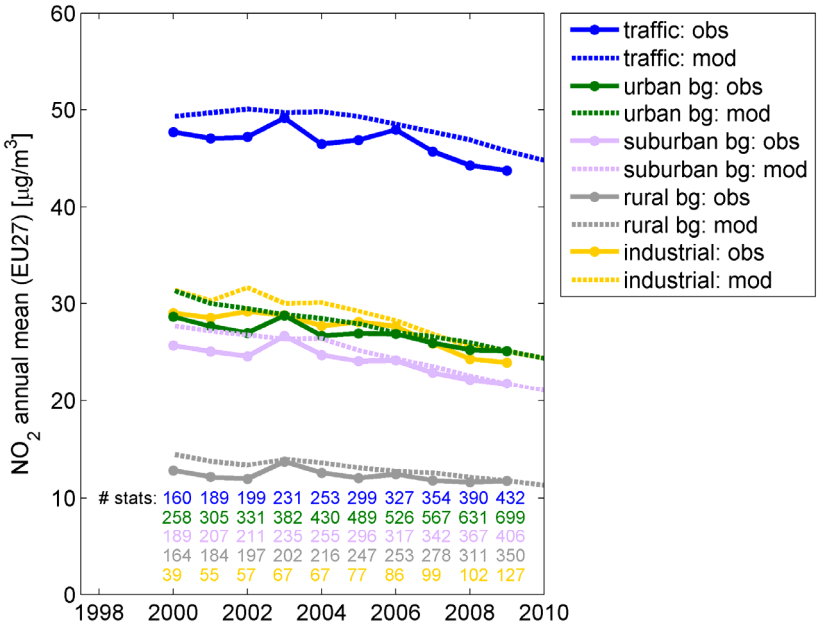

Figure 3.6: Observed vs. modelled annual mean NO_2 concentrations at measurement stations, averaged over the EU27 for different station categories. The number of measurement stations included in each year's average is shown at the bottom (the same set is used for observations and model).

In addition to validating the mean trend, also a station by station validation is essential. Due to the large number of stations covered, this needs to be done in a statistical way, e.g. as scatter plots. Since modelled concentrations are forced to match observations in 2009, the best validation is achieved by comparing model and observations in 2000, the earliest year covered by the model calculations. Figure 3.7 shows scatter plots of modelled and observed annual mean NO_2 concentrations for the year 2000 in the 16 EU countries with the highest numbers of reporting stations in AirBase. Concentrations are shown for all AirBase measurement stations that operated both in the base year 2009 as well as in 2000 and which are covered by our modelling scheme. For background stations (shown in black) there are no further requirements than sufficient observational data coverage (>80%), while for traffic stations (shown in red) the usual selection criteria regarding availability of roadside NO_x and background NO_2, NO_x and O_3 are applied. As apparent from the figure, modelled values are in excellent agreement with observations in most countries, although some scatter is encountered. The scatter is a direct result of station-specific characteristics which are inherently missed in our modelling scheme, since national emission trends are applied to all

stations. This station-specific uncertainty is discussed further in Section 4.1, and a way of dealing with it is proposed in Section 4.2.

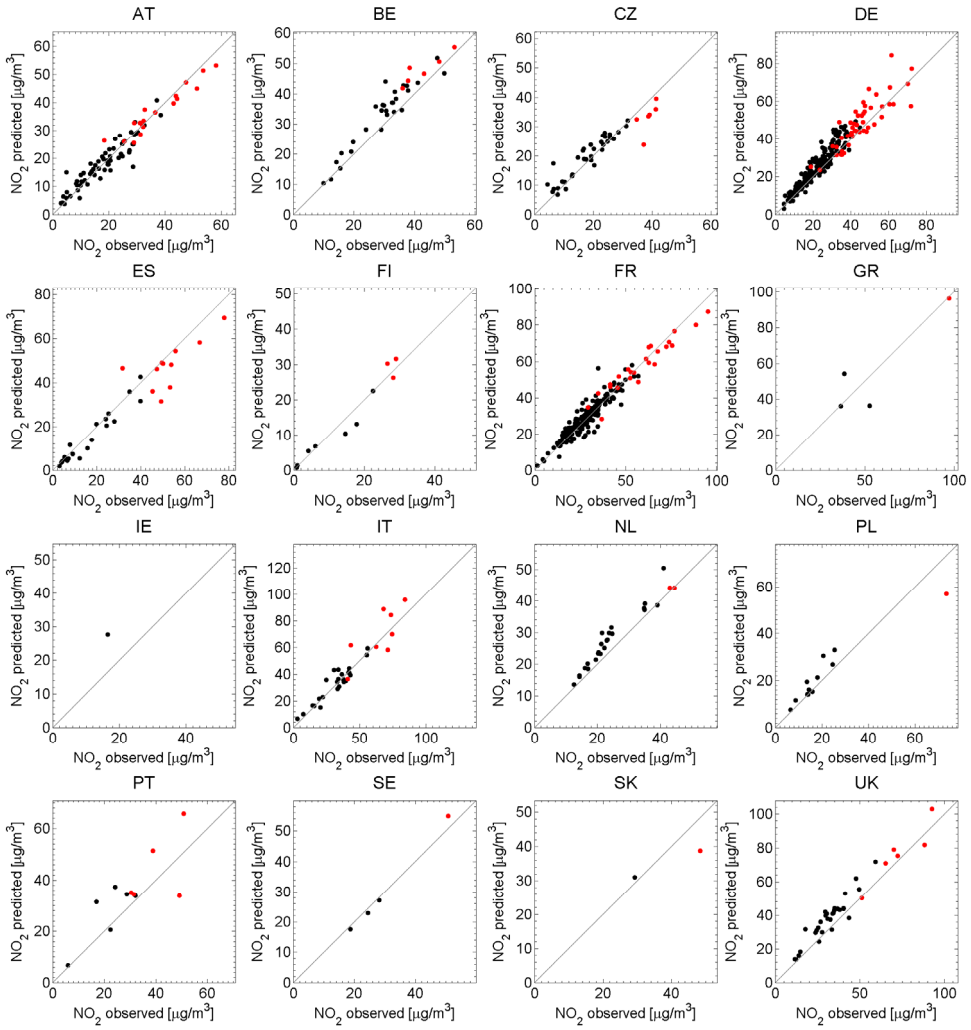

Figure 3.7: Scatter plot of back-casted (modelled) vs. observed NO_2 annual mean concentrations in 2000, for a subset of EU countries with at least two stations operational and modelled. Traffic stations are shown in red, while all other stations are shown in black.

3.2.2 PM10

In the same way as Figure 3.6, Figure 3.8 shows EU27 average annual mean PM10 concentrations for different station categories. The year-to-year variation in observed PM concentrations is considerably higher than in the case of NO_2, owing to the larger sensitivity of PM to meteorological variability (e.g., increased domestic heating emissions in colder winters, increased re-suspension of dust in hot summers, episodes of stagnant conditions during winter or episodic long-range transport of Sahara dust to Europe, episodic secondary inorganic aerosol).

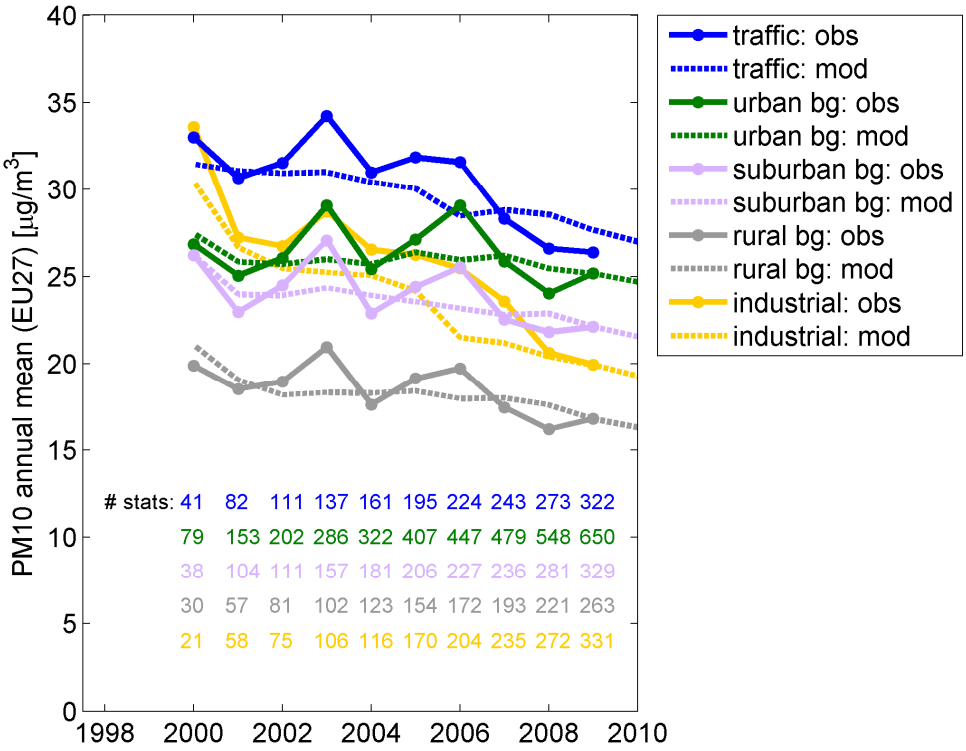

Figure 3.8: Annual average PM10 in the EU27, measured vs. modelled values at all analysed AirBase stations grouped into station categories. Numbers of stations available in each category and year are listed at the bottom.

These variations cannot be expected to be reproduced in our modelling scheme, which relies on 2006-10 average long-range transport and 2009 urban scale meteorology. The observed trend, on the other hand, is reproduced exactly at all station categories. All categories except the traffic stations use the urban background scheme. The slight over-estimation of traffic station concentrations by the model in the base year emerges from a few stations where the modelled PM2.5 increment exceeds the measured PM10 increment. Only minor improvements in urban, suburban and rural background PM10 concentrations are seen, due to the large contribution from stagnant domestic emissions. Thanks to improvements in vehicle exhaust after treatment technologies, concentrations at traffic stations have decreased more strongly. The strongest decreases, however, are seen at industrial stations, shifting them from the second highest to second lowest category, both in observations and model.

A station-by-station scatter plot validation of PM10 is shown in Figure 3.9, in the same way as for NO_2 in Figure 3.7. Here, 2001 is selected as the year for comparison, as the number of available stations increased sharply between 2000 and 2001 (numbers of stations available are listed at the bottom of Figure 3.8). The scatter of individual station results is considerably larger than for NO_2; nonetheless, in most countries a high correlation between observations and model results exists. A notable exception is Spain, where extremely high as well as extremely low observed values at several stations are not reproduced by the

model. This extreme spread seen in Spanish PM concentrations may be related to the strong influence of (local or Sahara) dust episodes, but further detailed station based analysis would be necessary to resolve this issue.

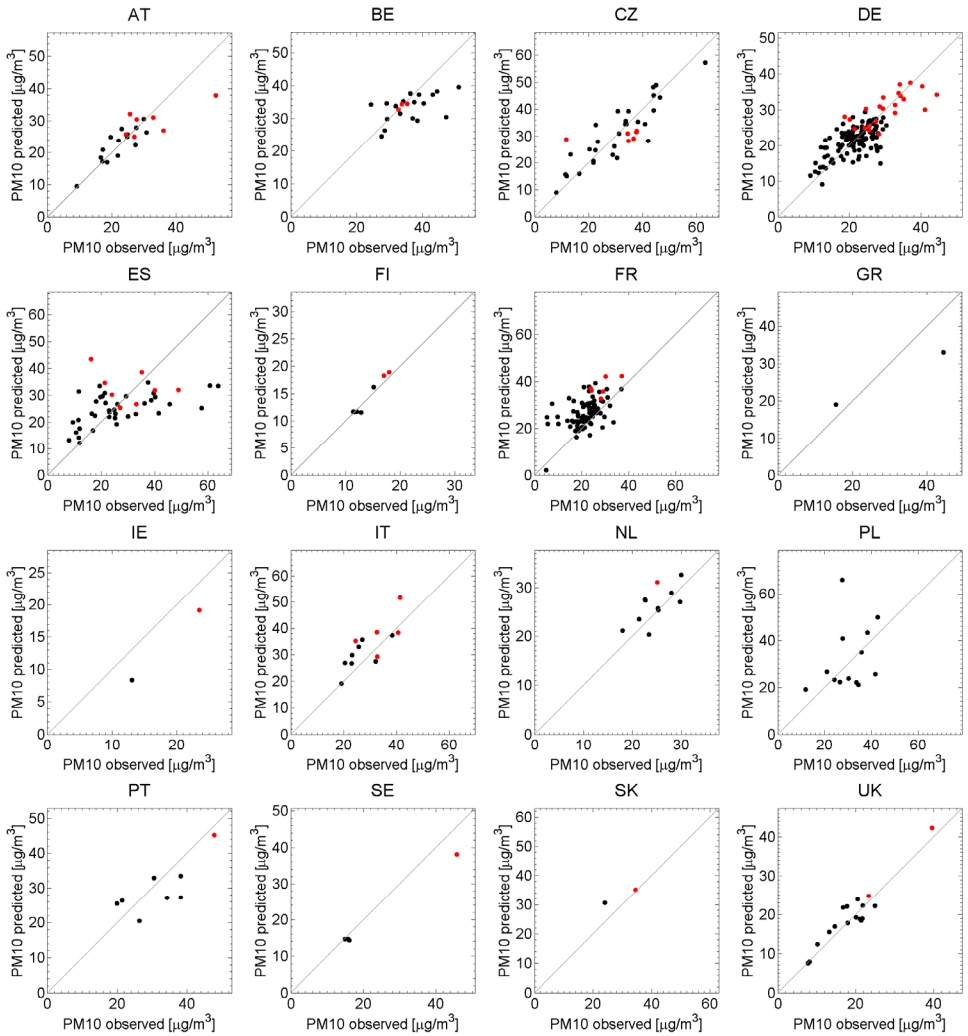

Figure 3.9: Scatter plot of back-casted (modelled) vs. observed PM10 annual mean concentrations in 2001, for a subset of EU countries with at least two stations operational and modelled. Traffic stations are shown in red, while all other stations are shown in black. 2001 is preferred over 2000 here as it marks the starting year of French monitoring data that has been made available to IIASA.

4 Uncertainties and robust solutions

The traffic station model is subject to different sources of uncertainty, both of systematic and statistical nature. Since it is based on observations, the quality of predicted concentrations is inherently connected to the quality of past observations feeding into the scheme.

Uncertainties in station-specific predictions arise, inter alia, from the fact that every station is assumed to follow national emission trends. This issue is discussed in Section 4.1 and leads to the formulation and validation of the more robust concept of compliance statistics in Section 4.2. Nonetheless, systematic uncertainties inherent to the construction of the model remain, which are discussed and quantified to the extent possible in Section 4.3.

4.1 Station specific uncertainties

As mentioned above, each monitoring site has its own characteristics that distinguishes it from others, such as building layout around the station influencing diffusion characteristics, typical fleet composition (e.g., near-by bus lines), characteristic driving situations (free flow vs. regular stop-and-go, suburban highway vs. inner city lane), local restrictions (speed limits, low emission zones). Strictly speaking, each traffic station would require its own emission scenario. Given the number of traffic stations covered by our model, this task is clearly unfeasible. The abovementioned parameters are not known for most of the stations, and even less so is their predicted evolution in the future. Thus, our model approach takes a compromise: Site-specific diffusion characteristics (residence time of air in the street canyon) are estimated from past concentration measurements, but emission trends are only calculated on a per country base. Emissions at each monitoring site are expected to follow the national trends, which introduces a site-specific error whose magnitude reflects by how much the station parameters deviate from the country average.

Strictly speaking, our model predictions give an estimate of the concentration changes that would result from emission controls if local station characteristics were set to the national average and no additional local measures taken whatsoever. Therefore, station specific results are not useless – to the first order, each station may still be described by the ensemble mean – but require great care in the interpretation. More robust results may be obtained from a statistical analysis: in a larger sample of stations, statistically independent differences between stations tend to cancel out.

These considerations lead to the concept of compliance statistics as a robust measure, which is introduced in Section 4.2.

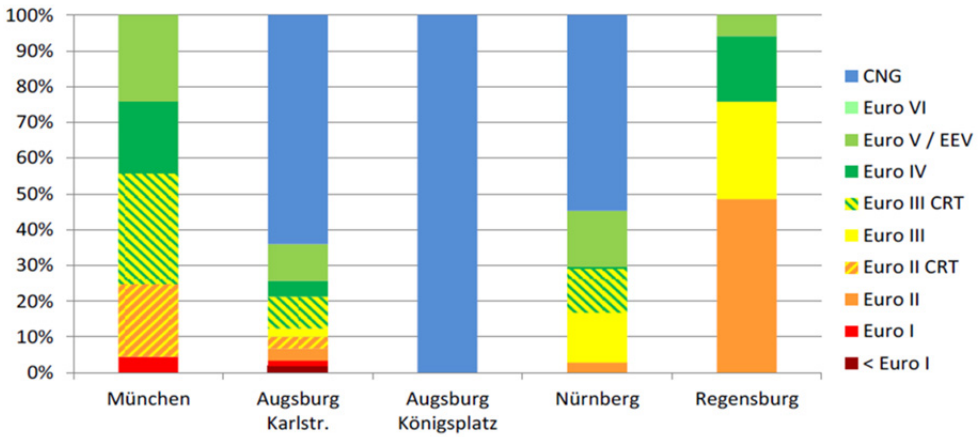

Figure 4.1: Mix of after-treatment technologies in bus fleets operating in different cities in Bavaria, Germany, in 2010 (Duennebeil et al. 2011)

4.2 Compliance statistics

The main purpose of our station-based modelling work is the analysis of likely compliance with limit values under future emission scenarios. In order to avoid the difficulties connected to station-specific predictions discussed in Section 4.1, we put the focus of our results on the ensemble of stations in a given country rather than each station individually. Stations are grouped into bands according to their predicted annual mean concentrations, resulting in a number of stations in each band as the final quantity to be analysed.

4.2.1 Concept

Compliance with limit values can be expressed through annual mean concentrations, as described in Section 2.2 (the limit value on daily mean PM10 concentrations is hereby replaced by an equivalent limit value on the annual mean of 30µg/m^3). Thus we group stations into three different categories, according to their predicted annual mean concentrations:

- annual mean more than 5µg/m^3 below the limit value: compliance likely
- annual mean within $\pm$5µg/m^3 of the limit value: compliance uncertain
- annual mean more than 5µg/m^3 above the limit value: compliance unlikely

Here, the range of 5µg/m^3 around the limit value does not mathematically translate into a distinct likelihood range, but is a chosen in the order of magnitude of typical year-to-year fluctuations observed.

For an individual station, the membership in one of the three categories gives a more reliable forecast quantity than an exact concentration, which is to a certain degree influenced by year-to-year changes in meteorological conditions. A

classification in the “compliance uncertain” or “compliance unlikely” categories provides strong indication that the station may still face difficulties in meeting the limit values, and additional local measures may be necessary to ensure compliance even under unfavourable meteorological conditions. On maps, the compliance categories may be used to point out geographical areas where difficulties remain.

The bigger advantage of the categorization of station results, however, lies in the prediction of ensembles of stations. In a sufficiently large ensemble, statistically independent differences in characteristics of individual stations may be expected to cancel out, so that the overall trend of the number of stations in a given compliance category in a given country appears as robust quantity. Naturally, this argument is the more valid the higher the number of stations per country and category is, which makes the model most suitable for countries with high numbers of critical or exceeding stations.

4.2.2 Validation

Validation of model results aggregated in compliance classes is done here by counting the numbers of stations in each class for each country. Figure 4.2 shows for the EU27 the evolution of station numbers in each of the compliance classes for the NO_2 limit value, as obtained from model calculations (dashed lines) and AirBase observations (dots).

Here it is more important than for the average concentrations shown in Figure 3.6 and Figure 3.9 to ensure that a common set of stations is compared. Recent years have seen large increases in numbers of monitoring stations in most Member States, so that the number of stations in each category increases over time although concentrations at individual stations may show a slight decline.

The number of stations in the “compliance likely” class dominates in most Member States; however, it is of least importance for the purpose of the modelling scheme. For enhanced readability of the graphs, the “compliance likely” category has been left out in Figure 4.2. Agreement between observations and model is excellent for most countries and years. Only in some Member States, the model faces difficulties in reproducing the trends, leading to, e.g., a moderate misattribution of stations between the “compliance uncertain” and “compliance likely” classes in Germany in the early 2000s. This may in part be connected to the increases in NO_2 exhaust emissions discussed in Section 3.2.1.

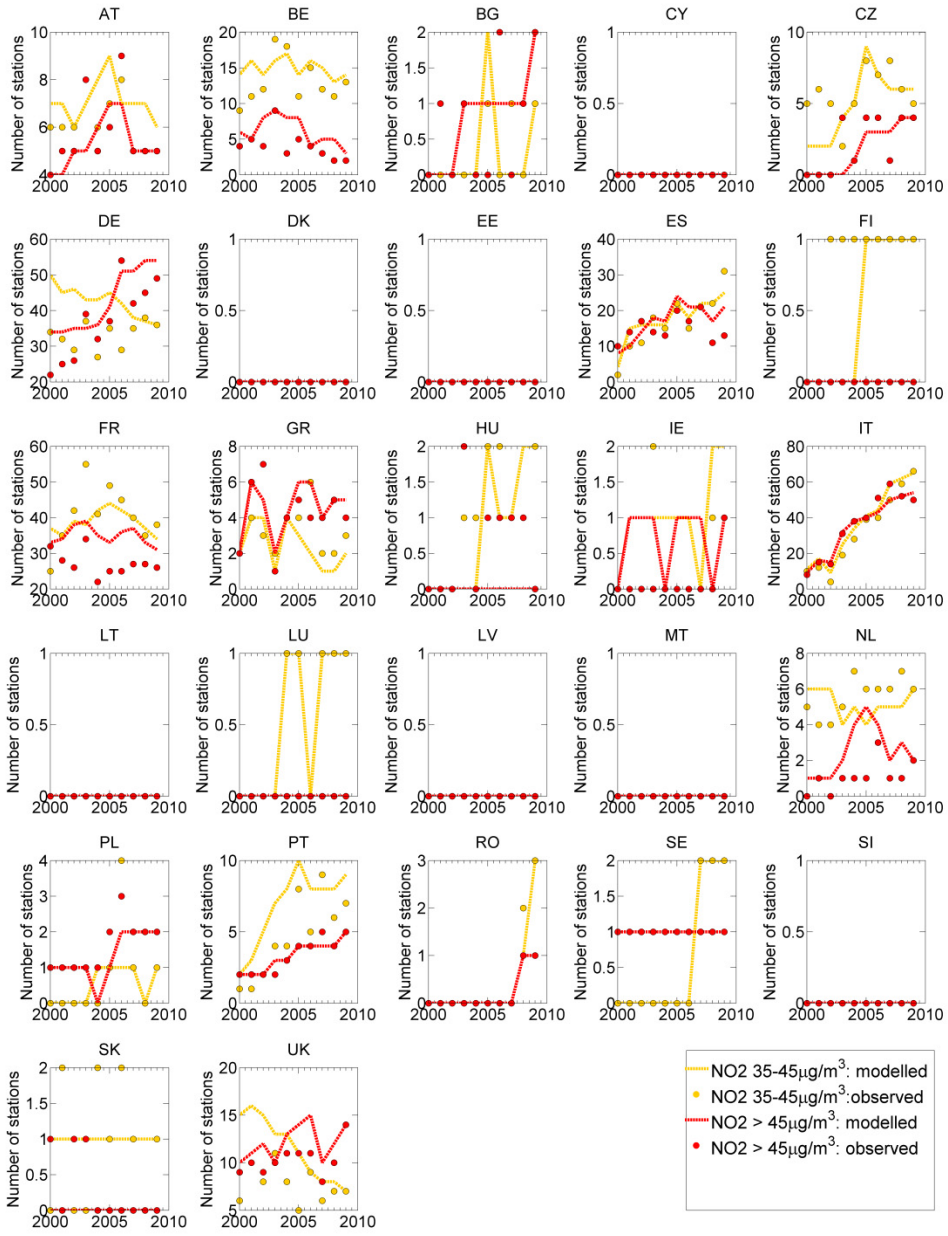

Figure 4.2: Numbers of stations grouped in different categories according to their annual average NO_2 concentration. Modelled values are shown as lines, whereas observed numbers are shown as dots. The comparison takes respect of the stations operative in each year individually, so that only stations from within the same overall set are compared each year.

The equivalent comparison for compliance with the PM10 limit value is shown in Figure 4.3. Although numbers may differ in individual years owing to varying meteorological conditions, the overall trend of station numbers in each category is reproduced well by the model, based – as all calculations – only on measured data in 2009. In some Member States (notably Portugal, Spain, Czech Republic, UK) the model faces difficulties in explaining strong reductions of concentrations at stations with large exceedances within a few years, leading to a mismatch between observed and modelled values in the "compliance unlikely" class.

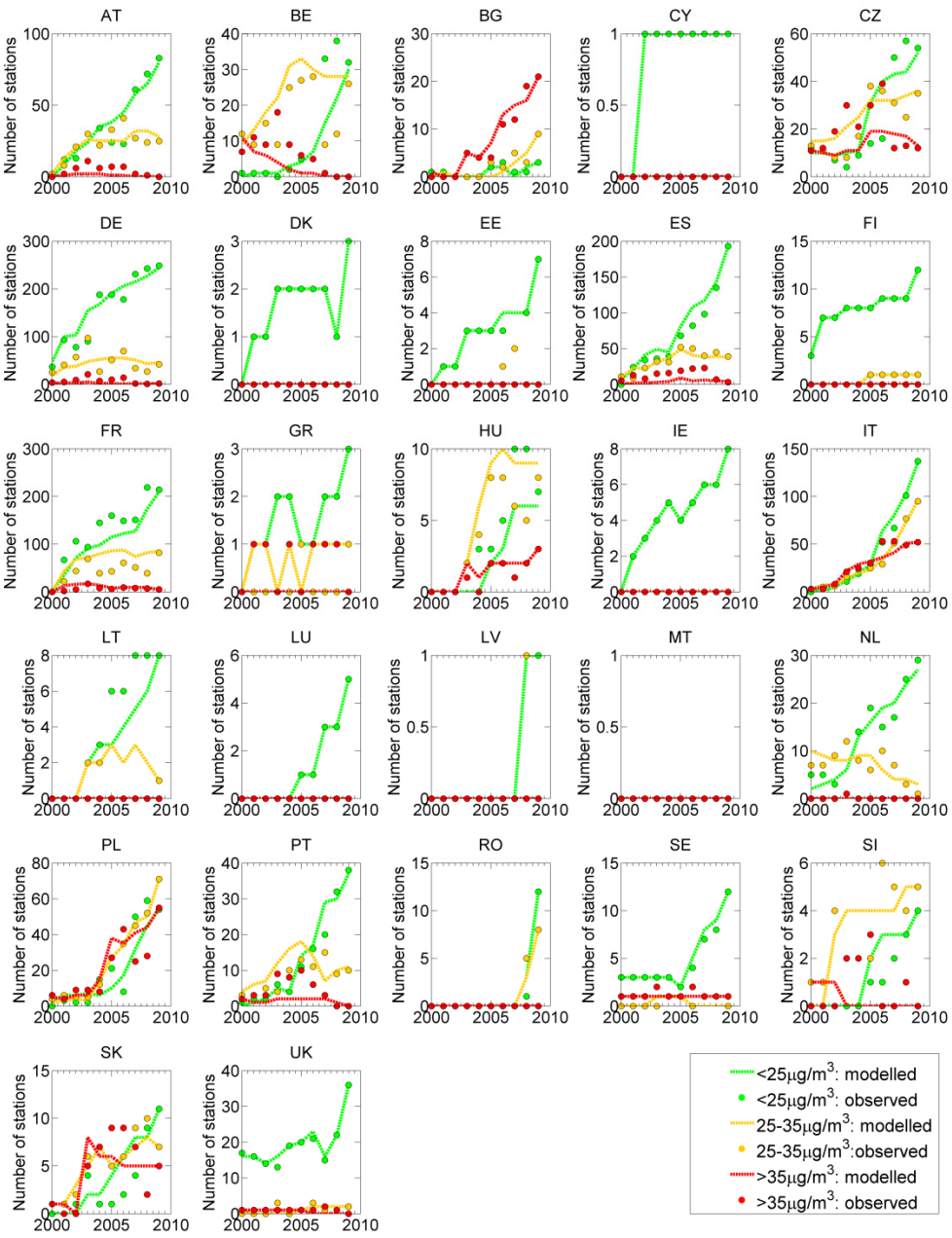

Figure 4.3: Numbers of stations grouped in different categories according to their annual average PM10 concentration. Modelled values are shown as lines, whereas observed numbers are shown as dots. The comparison includes stations operative in each year individually, so that only stations from within the same overall set are compared each year.

Compliance statistics such as shown in Figure 4.2 and Figure 4.3 are the most robust result of the model calculations, which will be provided for future scenarios. To avoid mis-interpretation, the following points should be taken into account:

- The numbers of stations in the "compliance unlikely" and "compliance uncertain" classes do not necessarily represent the numbers of exceeding

stations reported by Member States in the past, since the data requirements inherent to our modelling scheme restrict the set of stations covered.

- In the past, the increasing trends seen in Figure 4.2 and Figure 4.3 are to a large degree a consequence of increasing numbers of stations entering service. For predictions of the future, the set of stations is frozen at the base year 2009, leading to an artificial trend change in the base year. If new stations at hotspots continue to be opened, declines in absolute exceedance station numbers will take place more slowly than predicted by our scenario calculations.

4.3 Systematic uncertainty

While statistical differences between individual AirBase stations can be compensated by analysing aggregated compliance statistics as introduced in the previous section, systematic sources of uncertainty remain in the model. In this section, we list and quantify them to the extent possible, in particular with respect to the question whether they may cause biases in future predictions.

Key sources of systematic uncertainty are:

- Choice of base year: The choice of 2009 as a base year for the traffic station scheme is arbitrary and corresponds to the meteorological year for which the CHIMERE model simulation was carried out, as well as the latest year for which the AirBase observational data set was available at the time when the model development was started. Given the inter-annual variation in roadside NO_2 and PM10 concentrations from changing meteorological conditions or traffic volume, predicted NO_2 and PM10 levels depend on this choice to a certain extent. The range of NO_2 predictions starting from five different base years (2005-2009) is shown in Figure 4.4. Here, station specific parameters (τ and background representativeness adjustment) were derived for each base year individually, while emissions and long-range transport coefficients were left unchanged in the scenario analysis. Results are shown as numbers of stations in categories exceeding the limit value by more than $5\mu g/m^3$ ("compliance unlikely", red) and within $\pm 5\mu g/m^3$ of the LV ("compliance uncertain", yellow). Solid lines correspond to the results obtained with base year 2009, as published in the TSAP Impacts Report (Amann et al. 2012a), while shaded areas indicate the range spanned. Since the sets of available stations differs for different base years, station numbers for earlier base years have been scaled to match in 2009 the numbers obtained with base year 2009. Although the bandwidth of results is considerable for some countries, the general trend is confirmed. In particular, predicted numbers of stations in the "compliance unlikely" class seem robust, with only little spread in countries with high numbers of stations (DE, FR, IT, ES). The spread in station

numbers close to the limit value is considerably higher for the case of PM10, as shown in Figure 4.5. Roadside PM10 is affected more strongly than NO_2 by the interannual variations in local meteorology. Results are difficult to interpret, however, since the spread is increased by the fact that station numbers are scaled to match for 2009. Typically, station numbers are increasing from 2005 to 2009, and hence differences are also enlarged in this figure.

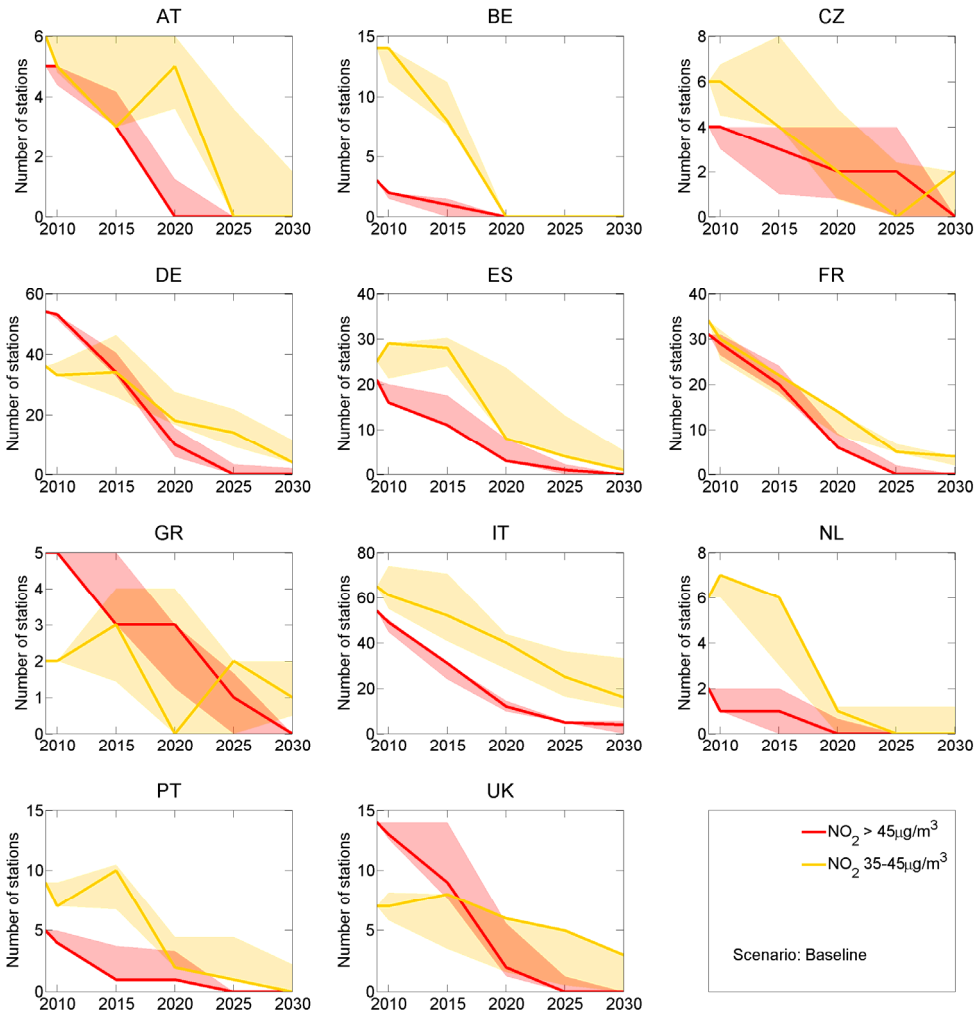

Figure 4.4: Range of predicted numbers of NO_2 stations in the "compliance unlikely" and "compliance uncertain" bands for five different choices of base year for the analysis. Solid lines correspond to base year 2009. Results obtained with other base years have been scaled to match the numbers for base year 2009 in 2009. Emission scenario: TSAP CLE (Dec 2012).

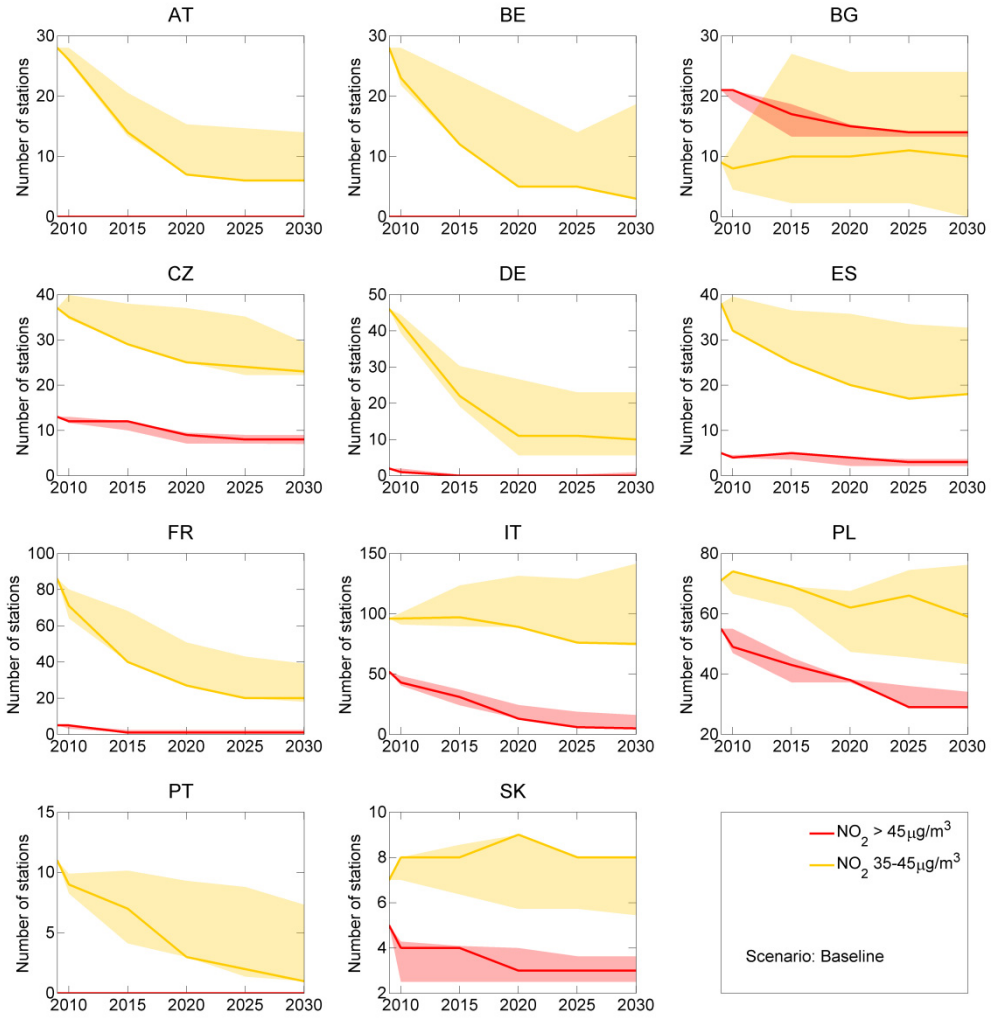

Figure 4.5: Range of predicted numbers of PM10 stations in the "compliance unlikely" and "compliance uncertain" categories for five different choices of base year for the analysis. Solid lines correspond to the results obtained with base year 2009. Results obtained with other base years have been scaled to match the numbers for base year 2009 in 2009. Emission scenario: TSAP CLE (Dec 2012)

- Choice of meteorological year for long-range transport, uncertainty about future meteorological conditions: Meteorological conditions vary between years. A quantification of the impacts of the interannual meteorological variability on long-range transport patterns is beyond the scope of this analysis. Effects of meteorological variability within cities leading to different mixing conditions are already contained in the analysis referring to different base years. Effects of changing long-range and transboundary transport could be quantified with transfer coefficients for different meteorological years. However, since urban background values used in the traffic station downscaling are adjusted to observations in the base year, the influence of different transfer coefficients is small.

- Linearity: A systematic source of uncertainty is connected to the assumptions of linearity underlying the representation of long-range transport and chemistry through transfer coefficients. Linear dependence of concentration increments on low-level urban emissions is also assumed in the urban background module.

- Measurement uncertainty, data issues: As the modelling scheme is based on observations, uncertainty in the AirBase observations is directly propagated into the model. Figure 4.6 shows a comparison of PM10 concentrations measured with two different devices at several measurement stations.Each dot represents a measurement made at the same time and location (in 18 European countries) by two instrumental devices: a JRC reference gravimetric sampler on the one hand and a monitoring network instrument on the other. Measurements have been collected within a period of 15 days in the frame of the European PM QA/QC programme (Lagler et al. 2011). While there is no absolute bias visible, the scatter induced only by the different devices is considerable. A more systematic problem is caused by different measurement techniques in use, which are not completely consistent (Hauck et al. 2004). The reference measurement technique is gravimetric, while also Tapered Element Oscillating Microbalance (TEOM) and Beta ray attenuation devices are widely used in some Member States. Usually a correction is applied to compensate for the underestimation of semi-volatile particles by the TEOM device. However, different correction methods (if any) are applied in different Member States, but not reported in a standardized way. Introduction of new correction factors, as for example done in France in January 2007 (AirParif 2011) causes systematic deviations in the measured values that affect the inter-comparability of values between different regions and years. In our model, we use the AirBase data as reported in the base year 2009. For the trend validation shown in Section 3.2, a simple correction is applied to French TEOM data measured before 2007.

- Choice of background stations: Unsuitable choices of background stations can have a considerable effect on the estimate of station parameters as well as on the magnitude of the roadside concentration increment. Our modelling scheme relies on the station classification provided by AirBase. Misallocation between background and traffic increment may result in a wrong roadside concentration trend, as too much or too little emphasis is put on the evolution of urban driving emissions.

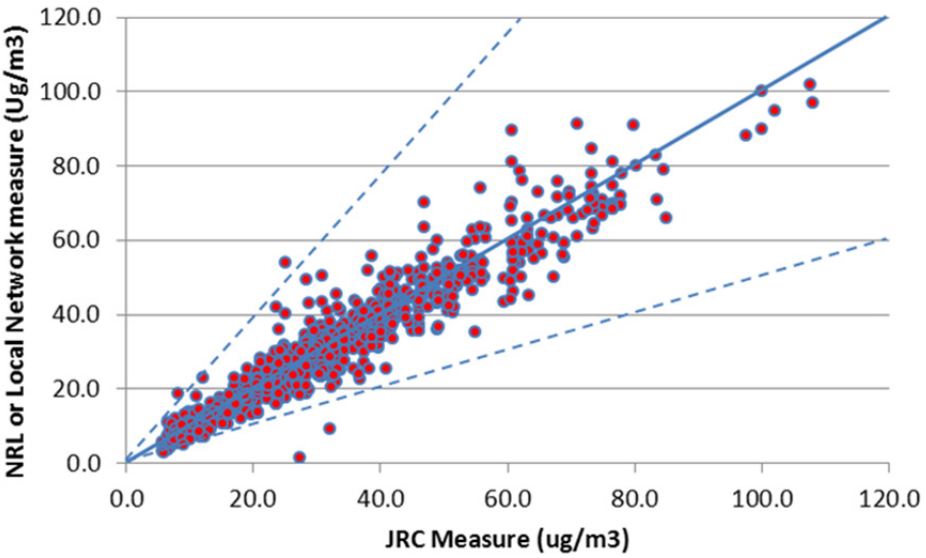

Figure 4.6: PM10 concentrations measured with two devices at several measurement stations: value measured with the calibrated JRC device (x axis), and the value measured with the local device at the same location and time (y axis). Figure courtesy of JRC Ispra.

- Model simplifications: Urban background scheme. The assumption that urban background NO_2 is in chemical equilibrium with NO_x and O_3 and not influenced by the share of NO_2 in NO_x emissions is not completely fulfilled in practice. Thus, large changes in the NO_2/NO_x emission ratio would lead to differences between urban background NO_2 and NO_x trends, which are not captured in the model. In case of increasing NO_2/NO_x emission shares, the model calculates a too negative NO_2 urban background trend. Over the period 2000-2009, a doubling of NO_2/NO_x emission shares results in deviations of modelled to observed concentrations of around 2µg/m^3 on average (Figure 3.6). NO_2 primary emission shares are expected to increase further in the future (Figure 2.15), although relative changes are smaller than in the past. Thus, modelled NO_2 concentrations for future years may have a tendency to be too optimistic by a few µg/m^3. In a policy context, we recommend focussing on the "compliance likely" category of stations as a measure for stations attaining the limit value.

- Model simplifications: NO_2 traffic station scheme. The traffic station scheme itself also induces uncertainty. In the NO_2 case, this mainly concerns the limited chemistry considered and the representation of the mixing process.

- Model simplifications - PM10 traffic station scheme. For PM10 the partitioning of the traffic increment into PM2.5 and PM_{coarse} is rather crude (the assumption that PM2.5 is perfectly modelled, and the residual to observed PM10 is only PM_{coarse}), and the assumption that PM2.5 disperses like a gaseous

tracer unaffected by sedimentation and re-suspension is not completely fulfilled in reality. Furthermore, the quantification of the PM2.5 increment via NO_x bears inherent uncertainty as it requires NO_x and PM2.5 emission factors to be consistent. National and urban emission factors differ in their PM2.5/NO_x emission ratios for some countries, with national numbers matching some of the available observations of PM2.5 increments better than using estimates of urban ratios. This leads to an overestimate of the PM2.5 increment and consequently underestimate PM_{coarse} increments in some countries (notably Germany). Thus, the PM10 traffic increment may be influenced too strongly by declines in PM2.5 emissions, while the small increases in PM_{coarse} are under-estimated, leading to a too fast decrease. A sensitivity study with national emission ratios results for 2030 in 1-2µg/m^3 higher concentrations than calculations based on urban ratios. Nonetheless, we employ urban emission factors for the PM2.5 increment calculation for the sake of consistency.

5 Discussion and Conclusions

The modelling scheme introduced in this report provides for the first time an extension of the GAINS model to estimate future NO_2 and PM10 concentrations at specific measurement stations. It follows a hybrid approach by combining bottom up modelling and observations reported in the AirBase data base for the year 2009. All types of measurement stations, in particular including roadside hotspot stations, are covered for the whole EU28, to the extent the data availability warrants. With the selection criteria that the model scheme infers, the model is able to provide calculations for 2015 NO_2 stations and 1902 PM10 stations (of a total of 2671 NO_2 stations and 2267 PM10 monitoring stations in AirBase 2009 with >80% data coverage). Among these modelled are 309 of 436 stations with annual mean NO_2 >40µg/m^3 and 494 of 613 stations with annual mean PM10 > 30µg/m^3 (315 of 387 if natural dust fields taken from the EMEP model are subtracted); in other words, we are able to provide scenario calculations for 71% of the NO_2 and 80% of the PM10 stations that violate the respective limit values in the 2009 AirBase data set (for PM10 the equivalent limit value of 30µg/m^3).

Although the model is able to explain a large fraction of observed urban background concentrations, EU-wide, 38% of PM10 at urban background stations remains unexplained (negative bias of 38%), translating into a fraction of about 21% unexplained PM10 at roadside stations. There are indications that the unexplained share is mostly PM_{coarse}, for which emissions are not well quantified, since natural dust emissions and road dust re-suspension play a significant role. In the absence of better knowledge, we assume the unexplained component to remain constant. For NO_2, the unexplained fraction is smaller on average: 73% of urban background NO_2 is explained, and due to the larger share of the local traffic increment, only 5% of roadside NO_2 remains unexplained. However, these numbers are subject to significant differences between and within Member States: in several large cities the urban background is over-predicted by the current approach. While unexplained components may be attributed to missing (natural) emissions, the interpretation of over-predicted NO_2 is not straightforward: possible reasons include spatial mis-allocation of emissions, non-linear relationships between emissions and concentration increments, or a wrong partitioning of NO_x into NO and NO_2 in the CHIMERE model. Over-predicted concentrations in the base year are corrected by a factor, so that the same relative trend as predicted from source-receptor relations and downscaling to the urban background is applied. As shown in Section 3.2, this results in modelled urban background trends that agree well with observations.

For the 432 NO_2 and 323 PM10 traffic stations contained in the set of modelled stations, the roadside increment scheme is applied on top of the urban background. In view of the size of the task, we apply a simple box model that is constrained by the actual observations in AirBase. Only basic NO_x-O_3 chemistry is taken into account for the NO_2 scheme, and in the PM10 traffic station scheme the

treatment of the fine fraction of the PM roadside increment is idealized. Station specific dispersion characteristics (mixing time τ in the NO_2 scheme, NO_x dispersion relation for PM2.5) are taken into account as far as they may be determined from the observations themselves, but station-specific emission characteristics are ignored. A detailed assessment of local conditions for each station is neither feasible (due to time constraints) nor possible (due to lack of data). Hence, we stress that this modelling scheme cannot replace detailed street canyon dispersion modelling at different hotspot sites, but is rather intended to complement detailed site specific studies. It provides a comprehensive framework for the assessment of compliance with limit values that is consistent both with observations and GAINS regional-scale calculations for future emission scenarios.

In this simplified modelling scheme, site-specific concentration predictions must be viewed with caution: They quantify effects of national and EU wide emission controls, but are ignorant of local peculiarities, which have had a significant influence on concentration levels in the past and will continue to do so in the future.

We suggest that statements about compliance of ensembles of stations provide a more robust result, as statistically independent differences in local trends (fleet composition, driving patterns) tend to cancel out at the aggregated level. For this purpose, stations are grouped into three categories according to their predicted annual mean concentrations in a respective year: Stations more than 5µg/m^3 below the limit value are considered likely to comply, stations within 5µg/m^3 of the limit value are considered uncertain to comply, and stations exceeding the limit value by more than 5µg/m^3 are considered unlikely to comply. The 5µg/m^3 margins are arbitrarily set and are inspired by the inter-annual variability of roadside concentrations due to meteorology. Since Member States are entitled to subtract from measured PM10 the contributions of long-range transport of dust and sea salt when determining compliance with limit values, we approximate this by subtracting the appropriate fields obtained from EMEP model runs for 2009. As shown in Chapter 3 as well as Section 4.2.2, the model is able to reproduce the observed trends both in terms of concentrations and compliance statistics. While the latter are the more relevant quantity for policy implications, their interpretation deserves caution. Strong increases in the numbers of stations violating limit values in the past are not necessarily related to increasing concentrations, but were to a large degree caused by increasing numbers of operational stations. At the majority of stations, declining concentrations have been observed, which are expected to continue in the future.

As many traffic stations show currently concentrations only slightly above the limit value, moderate decreases of concentrations are predicted to lead to disproportionally larger decreases in the number of stations violating the limit value. However, as long as concentrations are close to the limit value, variability in meteorological conditions, changes in traffic flow patterns, or temporary local

sources such as construction sites, may still lead to massive violations of limit values. Scenario calculations using the site-specific modelling scheme have been presented in the TSAP Impacts Reports (Amann et al. 2012c; Amann et al. 2012d), demonstrating the usability of the approach for scenario analysis. Different levels of ambitions in terms of emission controls were clearly shown to have different effects on the compliance situation with air quality limit values.

The downscaling approach presented in this paper has been developed to estimate impacts of future emission changes on the compliance with air quality limit values. It is, however, not appropriate for calculating population exposure, in particular for health impact assessments.

For this purpose, population exposure should be estimated for the urban background level, which corresponds better to calculated 7km grid average concentrations. This is done in the GAINS model with the same formulation as described in Section 2.3 (only PM2.5, no adjustment to observations).

Annex

A. The 7km emission inventory

The gridded distribution of anthropogenic emissions used for this exercise are provided by INERIS, they are based on a merging of databases from:

- TNO 0.125×0.0625 emissions for 2007 from MACC
- EMEP 0.5×0.5 for 2009
- emission data from the GAINS database
- INERIS expertise on re-gridding with various proxies (population, landuse, LPS data)

First the large point sources (LPS) from the fine scale (0.125×0.0625) TNO-MACC emissions data for 2007 were added to surface emissions to get only one type of emissions. For the various activity sectors the processing steps were the following:

SNAP 2: The country emissions were re-gridded with coefficients based on population density and French bottom-up data, the methodology was extrapolated to the whole of Europe. For PM2.5, the annual EMEP totals were kept except for the countries CZ, BA,BE, BY, ES, FR, HR, IE, LT, LU, MD, MK, NL, CS, TR. For the rest, PM2.5 emissions from GAINS were used. Additional factors were applied on Polish regions (×4 or ×8) for PM2.5 and PM10 emissions.

SNAP 3,7,8,9,10: TNO-MACC emissions were used as proxy to regrid EMEP 0.5°x0.5° annual totals

SNAP 1,4,5,6: EMEP 0.5°x0.5° emissions were regridded by adequate proxies (“artificial landuse”, EPER data for industries)

For countries where MACC-TNO emissions are not available EMEP 0.5×0.5 emissions are used (Iceland, small countries, Asian countries).

This inventory is interfaced with the CHIMERE model using chemical speciation and adequate temporal profiles. The procedure is fully documented in Menut et al. (2012).

B. CHIMERE CTM and its modifications for this exercise

The CHIMERE Chemistry Transport Model (CTM) has been described by Schmidt et al. (2001), Vautard et al. (2005), Bessagnet et al. (2008). CHIMERE includes all relevant gas phase and aerosol chemistry (both inorganic and organic secondary

aerosol formation). Here we use a resolution of 0.125° (lon) × 0.0625° (lat) and 8 vertical levels with 2009 meteorology and emissions.

Several modifications to the CTM have been made to optimize the simulation of urban dispersion conditions:

- 3D meteorological variables were switched from WRF to ECMWF-IFS data, to avoid overestimation of wind speed and thus too fast dispersion of emissions within urban areas (Miglietta et al. 2012)
- To account for the urban canopy influence on meteorology, wind speed and vertical diffusion (Kz coefficient) were modified. In the first layer, the wind speed was multiplied by a factor 0.5 (detailed below).
- To avoid over-estimation of wood burning in cities, SNAP 2 primary PM emissions from biomass burning were re-allocated over rural areas (detailed in Appendix A).
- To give a more realistic representation of increased domestic heating emissions in winter, a temperature proxy ("degree-days") was used for the temporal modulation of SNAP 2 emissions.

Adjustment of meteorology in urban areas

The IFS model has a 0.25° horizontal grid spacing (T799) from surface to 0.1 hPa (91 levels in total). It delivers typical meteorological variables (temperature, wind components, specific humidity, pressure, sensible and latent heat fluxes) vertically and horizontally interpolated on the CHIMERE grid (8 levels). Some of the variables are also used to diagnose additional turbulent parameters such as the friction velocity and the vertical wind speed used to quantify the vertical diffusion.

However, the main limitation of such data is that the IFS regional scale data cannot represent correctly the urban scale meteorology observed in the urban canopy layer and the urban sub-layer. This is crucial as the urban canopy is affecting the wind circulation and the urban energy balance (Sarrat et al. 2006) that will directly impact the transport and the vertical diffusion of primary pollutant over cities (e.g. O3, NO2 and PM). In order to integrate the influence of the urban canopy on meteorology, the wind speed and the vertical diffusion (Kz coefficient) are modified in the CHIMERE version used for this study. Usually, operational meteorological observations are performed outside urban areas (e.g. airport) for representativeness reasons. Some study reveals large differences between urban and rural winds (Fisher et al. 2006) showing a wind speed ratio (rural/urban) up to a factor two. Another study shows that within the modelling case of Lisbon the ratio between wind speed inside the canopy and at the top of the urban sublayer was within the range 0.1 to 0.6 (Solazzo et al. 2010). For those reasons, the wind speed in the first CHIMERE layer was multiplied by a factor 0.5 to limit the advection and diffusion of primary emitted pollutants.

C. Station selection criteria

The modelling scheme is based on monitoring data provided to the AirBase database by the Member States. For a station to be considered in our modelling scheme, we require a data coverage of at least 80% of hourly NO_2 concentrations, or 80% daily PM10 concentrations, respectively. For a background station, this requirement is sufficient, i.e. all background stations with at least 80% data available in 2009 are covered by the prediction model.

For traffic stations (and industrial stations in the case of NO_2), data availability criteria are more restrictive: For the NO_2 model, roadside NO_x, background NO_2, NO_x and O_3 must be available; for the PM10 model, roadside NO_x, background PM10 and background NO_x is needed. For each of the measured concentrations involved, the 80% data coverage criterion is applied. For the NO_2 parameter estimation algorithm to work properly, the annual average weekly pattern must be defined for every hour of the week for all species involved. Often missing background concentrations are the reason for non-coverage of a station.

Background stations for an arbitrary traffic station x are selected according to the following rules:

1. Background stations with the same city name as x mentioned in the AirBase meta data and with the same area classification ("urban", "suburban", "rural") as x
2. Background stations with the same city name as x mentioned in the AirBase meta data but with a "lower" area classification than x (e.g. suburban background station y for urban traffic station x)
3. Background stations located within 20km of x, with the same area classification as x
4. Background stations located within 20km of x, with a lower area classification as x (e.g. suburban background for urban traffic station)

The model relies on station type and area classifications as provided to AirBase by the Member States. Rules 1 – 4 are applied in this order until at least one background station candidate is found. The consideration of the station area classification in the selection process is important to ensure that the background is as appropriate as possible for the traffic station, and unrealistic values are prevented. For this reason, traffic stations without area classification in the AirBase meta data are excluded from the data set (only very few stations concerned). Criteria 2) and 4) ensure that if there is no background station available that is representative of the same area type that x is located in, only stations representing more remote surroundings will be taken into account as substitute. Allowing the opposite case, e.g. taking urban background values measured in the centre of a large city as background for a suburban traffic station located in the outskirts, may result in background values close to or exceeding

roadside concentrations at x and thus an unrealistically small or even negative roadside increment, which will lead to a mis-estimation of roadside NO_2 trends.

Since there are fewer O_3 monitoring stations available in urban surroundings, for O_3 the area type is not taken into account in the selection process, so that as a first choice all O_3 background stations with the same city name are selected, and if none is available, all O_3 background stations within 20km.

For the PM10 traffic increment model, care is taken to select the same background station(s) for PM10 and NO_x if any are available measuring both pollutants. In addition, if such station pairs are found, only days on which all stations are operative enter the background concentration calculation. This may result in slightly different annual mean $[NO_x]$ and $[NO_x]_B$ concentrations being used in the NO_2 and the PM10 traffic station models, but this serves the respective models best.

The selection of stations used in the model is based entirely on the availability of data in 2009. When determining observed background concentrations in earlier years for validation purposes as shown in Chapter 3, the selection process is applied to every year individually. Stations may be out of service temporarily for maintenance purposes, new stations are opened and others are taken out of service. This may cause discontinuities in the time series of observed background values and thus inconsistencies in the comparison with backward modelled concentrations. Since the focus of the model is on the analysis of impacts of future emission scenarios, we accept this disadvantage for the past.

Complete lists of all AirBase monitoring stations covered by the model, for NO_2 and PM10 separately, are provided as a supplement to this report on the IIASA website (http://gains.iiasa.ac.at/TSAP).

References

AirParif (2011) La Qualite de l'air en Ile-de-France en 2010. AirParif, Paris, France

Amann M, Bertok I, Borken-Kleefeld J, et al. (2011) Cost-effective control of air quality and greenhouse gases in Europe: modeling and policy applications. EMS 26:1489–1501. doi: 10.1016/j.envsoft.2011.07.012

Amann M, Bertok I, Cofala J, et al. (2012a) TSAP-2012 Baseline: Health and Environmental Impacts. TSAP Report #6. International Institute for Applied Systems Analysis, Laxenburg, Austria

Amann M, Borken-Kleefeld J, Cofala J, et al. (2012b) Future emissions of air pollutants in Europe – Current legislation baseline and the scope for further reductions. TSAP Report #1. International Institute for Applied Systems Analysis, Laxenburg, Austria

Amann M, Borken-Kleefeld J, Cofala J, et al. (2012c) TSAP-2012 Baseline: Health and Envronmental Impacts. TASP Report #6. International Institute for Applied Systems Analysis, Laxenburg, Austria

Amann M, Borken-Kleefeld J, Kiesewetter G, et al. (2012d) Compliance with EU Air Quality Limit Values - A First Set of Sensitivity and Optimization Analyses. TSAP Report #8. International Institute for Applied Systems Analysis, Laxenburg

Amato F, Pandolfi M, Escrig A, et al. (2009) Quantifying road dust resuspension in urban environment by Multilinear Engine: A comparison with PMF2. Atmospheric Environment 43:2770–2780. doi: 10.1016/j.atmosenv.2009.02.039

Berkowicz R (2000) OSPM - A Parameterised Street Pollution Model. Environ Monit Assess 65:323–331. doi: 10.1023/A:1006448321977

Bessagnet B, Menut L, Curci G, et al. (2008) Regional modeling of carbonaceous aerosols over Europe—focus on secondary organic aerosols. J Atmos Chem 61:175–202. doi: 10.1007/s10874-009-9129-2

Bohn B, Rohrer F, Brauers T, Wahner A (2005) Actinometric measurements of NO2 photolysis frequencies in the atmosphere simulation chamber SAPHIR. Atmos Chem Phys 5:493–503. doi: 10.5194/acp-5-493-2005

Boulter PG (2005) A review of emission factors and models for road vehicle non-exhaust particulate matter. Report No. PPR065. TRL Limited, Wokingham, UK

Boulter PG, Thorpe RJ, Harrison RM, Allen AG (2006) Road vehicle non-exhaust particulate matter: Final report on emission modelling. Report No. PPR110. TRL Limited, Wokingham, UK.

Carslaw D, Beevers S, Westmoreland E, et al. (2011a) Trends in NOX and NO2 emissions and ambient measurements in the UK.

Carslaw DC, Beevers SD, Tate JE, et al. (2011b) Recent evidence concerning higher NOx emissions from passenger cars and light duty vehicles. Atmospheric Environment 45:7053–7063. doi: 10.1016/j.atmosenv.2011.09.063

Duennebeil F, Rehberger I, Lambrecht U (2011) Szenarien zur Entwicklung der NO2-Immissionsbelastung an verkehrsnahen Luftmessstationen in Bayern Teil 1: Immissionssituation im Jahr 2010 und Referenzszenarien für 2015 und 2020. 47.

Duering I, Baechlin W (2009) TENDENZEN DER NO2-BELASTUNG IM LAND BRANDENBURG. Ingenieurburo Lohmeyer GmbH & Co. KG, Karlsruhe, DE

Düring I, Bächlin W, Ketzel M, et al. (2011) A new simplified NO/NO₂ conversion model under consideration of direct NO₂-emissions. Meteorologische Zeitschrift 20:67–73. doi: 10.1127/0941-2948/2011/0491

Fisher B, Kukkonen J, Piringer M, et al. (2006) Meteorology applied to urban air pollution problems: concepts from COST 715. Atmos Chem Phys 6:555–564. doi: 10.5194/acp-6-555-2006

Gehrig R, Zeyer K, Bukowiecki N, et al. (2010) Mobile load simulators – A tool to distinguish between the emissions due to abrasion and resuspension of PM10 from road surfaces. Atmospheric Environment 44:4937–4943. doi: 10.1016/j.atmosenv.2010.08.020

Grice S, Stedman J, Kent A, et al. (2009) Recent trends and projections of primary NO2 emissions in Europe. Atmospheric Environment 43:2154–2167. doi: 10.1016/j.atmosenv.2009.01.019

Harrison RM, Jones AM, Gietl J, et al. (2012) Estimation of the Contributions of Brake Dust, Tire Wear, and Resuspension to Nonexhaust Traffic Particles Derived from Atmospheric Measurements. Environmental Science & Technology 46:6523–6529. doi: 10.1021/es300894r

Harrison RM, Yin J, Mark D, et al. (2001) Studies of the coarse particle (2.5–10 μm) component in UK urban atmospheres. Atmospheric Environment 35:3667–3679. doi: 10.1016/S1352-2310(00)00526-4

Hauck H, Berner A, Gomiscek B, et al. (2004) On the equivalence of gravimetric PM data with TEOM and beta-attenuation measurements. Journal of Aerosol Science 35:1135–1149. doi: 10.1016/j.jaerosci.2004.04.004

Knoerr W, Duennebeil F, Lambrecht U, Schacht A (2011) Aktualisierung ”Daten- und Rechenmodell: Energieverbrauch und Schadstoff-emissionen des motorisierten Verkehrs in Deutschland 1960-2030“ (TREMOD, Version 5.2) für die Emissionsberichtserstattung 2012 (Berichtsperiode 1990-2010). ifeu Institut, Heidelberg, Germany

Kupiainen KJ, Tervahattu H, Räisänen M, et al. (2005) Size and Composition of Airborne Particles from Pavement Wear, Tires, and Traction Sanding. Environ Sci Technol 39:699–706. doi: 10.1021/es035419e

Lagler F, Belis C, Borowiak A (2011) A Quality Assurance and Control Program for PM2.5 and PM10 measurements in European Air Quality Monitoring Networks. JRC, Ispra, Italy

Lohmeyer A, Duering I (2001) Validierung von PM10-Immissionsberechnungen im Nahbereich von Strassen und Quantifizierung der Feinstaubbildung von Strassen. Senatsverwaltung f. Stadtentwicklung Berlin, Saechsisches Landesamt fuer Umwelt und Geologie Dresden, Radebeul

Menut L, Goussebaile A, Bessagnet B, et al. (2012) Impact of realistic hourly emissions profiles on air pollutants concentrations modelled with CHIMERE. Atmospheric Environment 49:233–244. doi: 10.1016/j.atmosenv.2011.11.057

Miglietta MM, Thunis P, Georgieva E, et al. (2012) Evaluation of WRF model performance in different European regions with the DELTA–FAIRMODE evaluation tool. International Journal of Environment and Pollution 50:83–97. doi: 10.1504/IJEP.2012.051183

Ntziachristos L, Gkatzoflias D, Kouridis C, Samaras Z (2009) COPERT: A European Road Transport Emission Inventory Model. Information Technologies in Environmental Engineering - Proceedings of the 4th International ICSC Symposium Thessaloniki, Greece, May 28-29, 2009. Springer Berlin Heidelberg, pp 491–504

Ntziachristos L, Mellios G, Kouridis C, et al. (2008) European Database of Vehicle Stock for the Calculation and Forecast of Pollutant and Greenhouse Gases Emissions with TREMOVE and COPERT. Thessaloniki, Greece

Omstedt G, Bringfelt B, Johansson C (2005) A model for vehicle-induced non-tailpipe emissions of particles along Swedish roads. Atmospheric Environment 39:6088–6097. doi: 10.1016/j.atmosenv.2005.06.037

Sarrat C, Lemonsu A, Masson V, Guedalia D (2006) Impact of urban heat island on regional atmospheric pollution. Atmospheric Environment 40:1743–1758. doi: 10.1016/j.atmosenv.2005.11.037

Schmidt H, Derognat C, Vautard R, Beekmann M (2001) A comparison of simulated and observed ozone mixing ratios for the summer of 1998 in Western Europe. Atmospheric Environment 35:6277–6297. doi: 10.1016/S1352-2310(01)00451-4

Seinfeld J, Pandis S (1998) Atmospheric Chemistry and Physics - From Air Pollution to Climate Change. Wiley Interscience, New York

Simpson D, Benedictow A, Berge H, et al. (2012) The EMEP MSC-W chemical transport model–technical description. Atmos Chem Phys 12:7825–7865.

Solazzo E, Sabatino SD, Aquilina N, et al. (2010) Coupling Mesoscale Modelling with a Simple Urban Model: The Lisbon Case Study. Boundary-Layer Meteorol 137:441–457. doi: 10.1007/s10546-010-9536-6

Thorpe A, Harrison RM (2008) Sources and properties of non-exhaust particulate matter from road traffic: A review. Science of The Total Environment 400:270–282. doi: 10.1016/j.scitotenv.2008.06.007

Vautard R, Honore C, Beekmann M, Rouil L (2005) Simulation of ozone during the August 2003 heat wave and emission control scenarios. Atmospheric Environment 39:2957–2967.